DOI 10.1007/s10778-016-0730-1
International Applied Mechanics, Vol. 52, No. 1, January, 2016

FINITE-FIBER MODEL IN THE THREE-DIMENSIONAL THEORY OF STABILITY OF COMPOSITES (REVIEW)

A. N. Guz and V. A. Dekret

Results obtained using the three-dimensional linearized theory of stability of deformable bodies (TLTSDB) and the new so-called finite-fiber model for fibrous and laminated composites are reviewed and compared with the results previously obtained using the well-known infinite-fiber model. The article consists of two parts.

The first part is a short historical sketch of experimental and theoretical studies into the following two problems: (i) microbuckling of composites and (ii) failure or fracture of composites when microbuckling is the initial stage of the process. The applicability of the infinite-an d finite-fiber models to various composites is confirmed by analyzing experimental results obtained by various authors.

The second part is a brief review of theoretical results obtained using the TLTSDB and the finite-fiber model for fibrous and laminated composites. The buckling problem is solved for the following cases: one and two short fibers, a periodic row of short fibers, and short fibers near a free boundary. The influence of mechanical and geometric parameters of the composite components on the critical strain and buckling of reinforcement is analyzed. The results for the finite-fiber model were obtained by solving a plane problem and considering the prospects for solving spatial problems, which is very important

Keywords: composite materials, instability, internal structure, compression, infinite-fiber model, finite-fiber model, failure or fracture, approximate theories of stability of thin-walled plates and rods, three-dimensional linearized theory of stability of deformable bodies, fibrous and laminated composites, critical strain, finite-difference method, reference scheme, discrete models, one and two short fibers, periodic row of short fibers, near-surface short fibers

Introduction. The literature on the mechanics of composites and fracture mechanics currently recognizes the paper [39] published in 1960 to be the first to describe the phenomenon of microbuckling of fibers as a type of fracture of a unidirectional composite under compression. Thus, the microbuckling of a composite under compression is the initial stage (start) of fracture. In subsequent years, the phenomenon of microbuckling in laminated and fibrous composites compressed along the reinforcement was addressed in numerous studies.

For the purpose of theoretical studies, a number of models of various level of accuracy and consistency based on the general infinite-fiber model were proposed. This model deals with a periodic (along the reinforcement axis) buckling mode, which makes it possible to study materials with unbounded matrix reinforced with infinitely long fibers and, thus, to neglect the effect of the boundary conditions at the ends of fibers. This model was validated for a number of composites and, naturally, it is applicable to relatively long fibers. The infinite-fiber model is discussed in more detail in Sec. 1. It should be noted that this model was applied in almost all studies on microbuckling in composites, beginning with the paper [41] published in 1965.

The infinite-fiber model is inapplicable to relatively short (along the reinforcement axis) fibers because the buckling modes are affected by the ends of the fibers. In this case, it is necessary to apply the finite-fiber model and to consider specific

S. P. Timoshenko Institute of Mechanics, National Academy of Sciences of Ukraine, 3 Nesterova St., Kyiv, Ukraine 03057, e-mail: guz@carrier.kiev.ua. Translated from Prikladnaya Mekhanika, Vol. 52, No. 1, pp. 3–77, January–February, 2016. Original article submitted October 17, 2014.

boundary conditions at the fiber ends. Naturally, this model does not assume periodicity (along the reinforcement axis) of the buckling mode and it is determined by solving the appropriate strictly formulated problem and taking into account the boundary conditions at the fiber ends. The finite-fiber model was applied to solve a plane problem in the papers [9, 52] published in 2000. Later, this approach was used to study microbuckling in composites in the following cases: one fiber, two fibers, a periodic row of fibers, and fibers near the boundary of the material. Results obtained using the finite-fiber model are detailed in Sec. 2.

A few words about the terminology. In this paper, we will use the terms "infinite-fiber model" and "finite-fiber model" with reference to both unidirectional fibrous composites and laminated composites. For the latter, it would be appropriate to use the terms "infinite-ply model" and "finite-ply model." To cover both unidirectional fibrous and laminated composite, it would be correct to use the terms "infinite-reinforcement model" and "finite-reinforcement model." We believe, however, that the terminology "infinite-fiber model" and "finite-fiber model" is more informative for experts in composite materials.

In this paper, we will discuss not only microbuckling in, but also fracture of unidirectional fibrous and laminated composites under compression. In this connection, we will give some remarks on the terminology used in the fracture mechanics of materials and structural members. By fracture is usually meant the propagation of one or several cracks; hence, fracture mechanics studies the fracture of materials and structural members in which one or several cracks propagate. By failure is meant the loss of load-carrying capacity by a material or a structural member that is mainly manifested not only as propagation of one or several cracks, but also as other mechanisms. This situation is studied by failure mechanics. By damage is meant the accumulation of dispersed growing or incipient cracks or other defects. Damage mechanics studies the laws (kinetics) of damage accumulation based on continuum models and a specially chosen damage indicator. This classification is certainly a matter of convention; yet, it is quite useful and informative for the analysis of various results in fracture mechanics, in the broad sense of this term.

Typical failure mechanisms in the internal structure of a composite under various loads are described in [8, Vol. 1, p. 46, Fig. 0.1], where further references are given. Typical failure mechanisms in the internal structure of unidirectional composites under various loads are schematized in [8, Vol. 1, p. 47, Fig. 0.2].

Images of typical failure mechanisms in composites compressed along the reinforcement (fibers) can be found in [8]; the same images are shown here, in Sec. 1. When a composite is compressed along the reinforcement, fracture is localized within narrow zones that can be modeled by cracks. In these zones, fibers collapse and break. Thus, in this situation, several failure mechanisms interact. Therefore, it may be stated that we deal with the phenomenon of "failure" studied by failure mechanics. For the sake of completeness, however, one may use both terms in this way: "failure or fracture" and "failure or fracture mechanics."

This completes the Introduction. Thus, the present paper consists of Introduction, Section 1, and Section 2.

In Section 1, we will analyze typical experiments on microbuckling in composites compressed along the reinforcement (fibers) and subsequent fracture initiated by the microbuckling. Also, we will briefly analyze approaches, problem formulations, models, problem-solving methods, and specific results obtained using the infinite-fiber model.

Section 2 briefly discusses theoretical results on stability in the internal structure of composites compressed along the reinforcement obtained by solving a plane problem using the finite-fiber model and the three-dimensional linearized theory of stability of deformable bodies (TLTSDB).

1. Analysis of Experimental and Theoretical Results. We will analyze experimental results on microbuckling in compressed composites followed by their fracture and theoretical results obtained using the infinite-fiber model.

1.1. Analysis of Experimental Results. Let us analyze experimental studies of the phenomena of microbuckling in compressed composites and experimental results on the fracture behavior of compressed composites.

1.1.1. Experimental Results on Microbuckling in Compressed Composites. It should be noted that microbuckling is not observed in homogeneous materials. It is only typical for composites (as for structurally inhomogeneous materials whose internal structure is described at different scales during analysis). The structural homogeneity or inhomogeneity of a material is mainly determined by the scale of the processes, which, in turn, is determined by the variability of fields of mechanical variables (stresses, strains, etc.) with the space variables.

In analyzing experimental results on microbuckling in composites, it is necessary to take into account the following. It is very difficult to experimentally observe (record) pure microbuckling in composites compressed along reinforcements (fibers, filler) because insignificant or significant fracture also occurs at the very beginning of microbuckling. In this connection, the existence of microbuckling in a compressed composite is usually proved by conducting special experiments.

Fibers (reinforcement) are placed in epoxy (or other) resin that is allowed to polymerize at certain temperature; after that the resin cools down to certain temperature and sets. In almost all cases, compression occurs as the matrix (resin, binder)

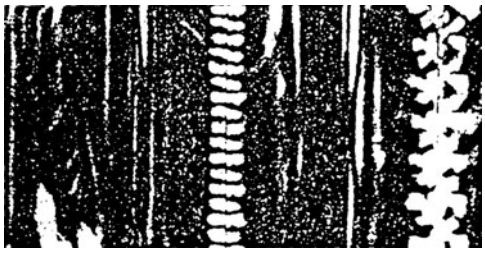

Fig. 1.1

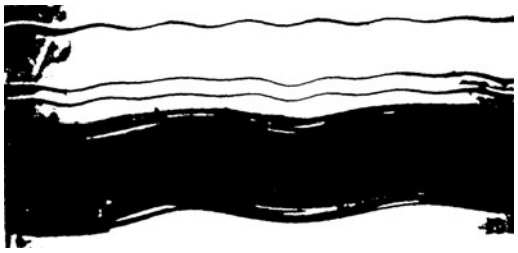

Fig. 1.2

shrinks upon setting or as the composite cools down. Since the thermal-expansion coefficient of the fibers and matrix, which are coupled, are different, the fibers are subject to compressive loads.

These experiments were conducted at various centers of science at various times. The results of such experiments have been published.

These experimental results were, apparently, reported for the first time in [26] in Russian (in 1967) and in [67] in English (in 1965). In this connection, we will discuss the results from [26, 67]. For example, Fig. 1.1 [26, Fig. 3.20] shows a photoelastic pattern for three E-glass fibers (diameters 0.13, 0.09, 0.013 mm) in an epoxy resin matrix polymerized at a temperature of 120°C. The photoelastic pattern is periodic (with a great number of periods), which is indicative of a sinusoidal (along the fibers) buckling mode. Later, related experimental results were obtained at many centers of science, using also other resin (matrix) curing methods.

We will now discuss, as an example, experimental results for thermochemically setting resin (matrix) in which glass fibers and strands floated before curing. These results for 0.01 mm glass fibers were published in [41] in 1982. Figure 1.2 [41] shows (50x magnification) results for separate fibers and a fiber strand after thermochemical curing of resin (matrix). It can be seen that the entire strand and individual fibers take on a well-defined periodic sinusoidal (along the fibers) shape after curing of the resin (matrix).

It should be noted that Figs. 1.1 and 1.2 (published in the second half of the 20th century) represent the microbuckling of composites reinforced with glass fibers 0.13, 0.09, 0.013, and 0.01 mm in diameter. Related experimental studies for composites reinforced with fibers made of other materials and compressed after shrinkage of resin (matrix) due to its curing or cooling have also been conducted now (in the beginning of the 21st century).

An example of experimental results for carbon fibers in a polymer matrix (epoxy resin) is the paper [60] published in 2004. Figure 1.3 [60] shows a periodic sinusoidal buckling mode with a great number of periods. The buckling mode in Fig. 1.3 (the scale in μm is indicated in the lower left corner) was recorded in [60] at the 68th second of cooling of the polymer matrix.

Along with the results for glass and carbon fibers in Figs. 1.1–1.3, experimental results on microbuckling in various composites have been published recently.

Thus, the above and related experimental results for quite long fibers in a matrix (binder) confirm that the phenomenon of microbuckling can occur in composites. The buckling modes in Figs. 1.1–1.3 are periodic (along the fibers) sinusoidal and have a great number of periods. In this connection, the boundary conditions at the ends of reinforcements (fibers) cannot strongly affect buckling modes and critical loads and strains. The above experimental results validate the long-fiber model.

As repeatedly mentioned above, the infinite-long model is, obviously, applicable to relatively long fibers (reinforcements). It may be a priori expected that the microbuckling modes in a composite reinforced with relatively short fibers is considerably different from the buckling modes in Figs. 1.1–1.3 corresponding to the infinite-fiber model. Let us consider, as an example, the experimental results on the stability of relatively short carbon nanofibers in a polymer matrix published in [69] in 2004. Figure 1.4 [69] shows buckling modes of two short carbon nanofibers, the scale in nm being indicated in the lower left corner of the figure. The buckling modes in Fig. 1.4 have nothing in common with those in Figs. 1.1–1.3. The buckling modes in Figs. 1.1–1.3 are sinusoidal (along the fibers) and have a great number of periods, while the buckling modes of short nanofibers in Fig. 1.4 can be approximated by sinusoids with one half-period. In this case, the critical loads and strains are strongly dependent on the boundary conditions at the ends of fibers.

Thus, the experimental results in Fig. 1.4 may be considered to validate the finite-fiber model.

We may now conclude that the infinite-fiber and finite-fiber models are experimentally validated, but they are applicable to different types to composites. For example, the infinite-fiber model is applicable to composites with relatively long

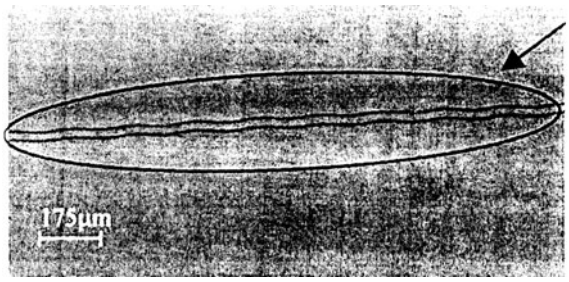

Fig. 1.3

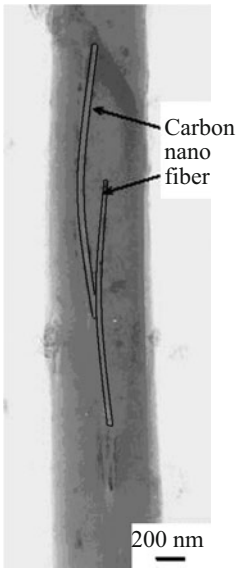

Fig. 1.4

fibers, while the finite-fiber model is applicable to composites with relatively short fibers. Note that the conclusions drawn from Figs. 1.1–1.4 apply only to the phenomenon of microbuckling in composites.

Remark 1.1. The experimental studies represented in Fig. 1.1–1.4 were specially set up (i.e., are model experiments) to prove the existence of the microbuckling phenomenon in composites. Taking a close look at Fig. 1.1–1.4, we can observe microbuckling in pure form, i.e., without signs of failure, because no separation of the fibers from the matrix can be seen. This situation appears quite important and should be given appropriate attention in analyzing the experimental results on the fracture of compressed composites in the next section.

Remark 1.2. Here we address various processes in mainly unidirectional composites compressed mainly, along the fibers, i.e., in the direction of preferential reinforcement. In continuum approximation, these composites, as well as cross-ply composites, are modeled by orthotropic homogeneous materials. Thus, we will use the orthotropic model to study compression along the axes of symmetry of materials. A similar situation occurs under loading of other types, as in compressed zones of various bent structural members and in other cases. When various structural members (rods, plates, and shells) are compressed along the axes of (geometrical and material) symmetry, the basic mechanism of structural failure is buckling.

In studying compression of composites along the fibers or, in the more general case, in the direction of preferential reinforcement, it may be a priori expected that fracture of composites (as well as structural failure of structural members under similar loading) starts with microbuckling. The above situation may be considered as the basic concept that should be taken into account in analyzing experimental results on the fracture of composites compressed along the axes of symmetry. This is discussed in the next section.

1.1.2. Experimental Results on the Fracture of Compressed Composites. Here we will analyze experimental results on compressed composites after fracture. These results are images of an already destroyed material that, naturally, do not show the initial stage (start) of fracture. Hence, no experimental studies have yet been made of the entire fracture process under compression, from microbuckling (initial stage (start) of fracture) in the composite to the fragmentation of the composite (final stage of fracture). Such studies have not also been made of most fracture processes in other materials under other types of loads.

Thus, we will analyze the fracture behavior of compressed composites using scaled-up images of an already destroyed composite. The experimental studies to be discussed are focused on composites the compressed along the axes of material symmetry (along fibers in unidirectional composites, in the direction of preferential reinforcement in cross-ply composites, and in the perpendicular direction to the plane of preferential reinforcement in cross-ply composites). We will analyze specific features of fracture behavior under loading of the type being considered.

It should be noted these specific features are observed in compression not only in the direction of preferential reinforcement, but also in the perpendicular direction. The above situation can be illustrated by results from the paper [1] published in 1968, such as Fig. 1.5 reprinted in the book [21, p. 110]. In [1], a glass-fiber laminate uniaxially compressed in the

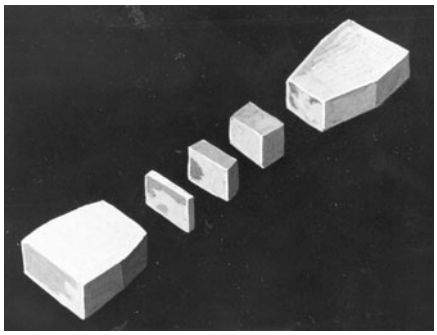

Fig. 1.5

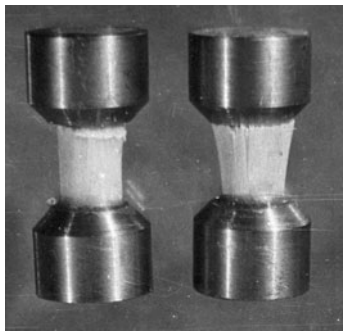

Fig. 1.6

Fig. 1.7

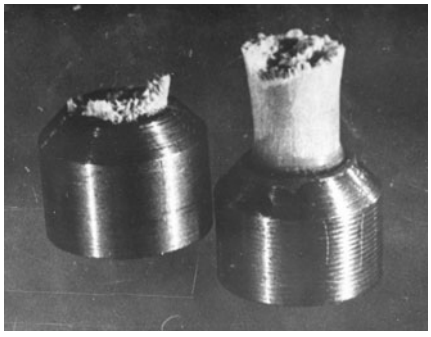

Fig. 1.8

perpendicular direction to the reinforcement plane was considered. Figure 1.5 shows that fracture occurred in planes perpendicular to the load direction, causing the material to fragment. Fracture of such composites along planes almost perpendicular to the uniaxial compressive load is a specific feature.

Results on the fracture behavior of unidirectional fiberglass-reinforced plastic specimens compressed along the fibers are presented in [57] published in 1969. These results were obtained at the Institute of Mechanics of the Academy of Sciences of the USSR (currently the S. P. Timoshenko Institute of Mechanics). Cylindrical specimens 10 mm in diameter and 45 mm in height and 15×15×70 mm prismatic specimens (Fig. 1.6) were cut out from glass-fiber-reinforced plastic plates made by winding over a metal mandrel followed by hardening under a press at a specific pressure of 1 MPa. NS-55/6 alkali-free glass fibers with wax emulsion as a sizer were used as reinforcements (filler), and EFB-4 epoxy-phenolic binder was used as a matrix. The fraction of the matrix by weight was 26.6%, the degree of polymerization being 89.9%. The techniques of making and testing the specimens are detailed in [8, Vol. 1, pp. 189–191; 57].

It should only be noted that the crushing of the ends of compressed specimens was avoided by putting metal rings on the specimens at their ends and filling them with cold-setting epoxy resin. As a result, the specimen length not covered by the rings was 1.5 to 2 of the linear dimension of the cross-section. Figures 1.7 and 1.8 show the fracture behavior of specimens of circular and square cross-sections, respectively. After fracture, the specimens were easily split into the two fragments shown in the figures. Note that fracture commonly occurred near the metal rings, which is possibly due to the initial local fracture caused by cutting extreme fibers.

The fracture (Fig. 1.6) of unidirectional fiberglass-reinforced plastic specimens compressed along the fibers propagates along planes almost perpendicular to the fibers and to the line of action of the compressive load.

Thus, the fracture of unidirectional fiberglass-reinforced plastic compressed along the fibers and compressed glass-fiber laminate compressed in the perpendicular direction to the reinforcement planes propagates along planes almost perpendicular to the line of action of the uniaxial compressive load. This situation is a specific feature of the type of fracture under consideration. Note that in both cases (Figs. 1.5–1.8), the specimens are compressed along the axes of material symmetry. Additional considerations on the fracture process can be found in [8, Vol. 1, p. 191].

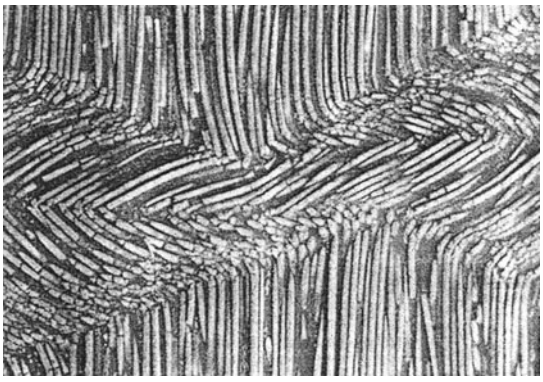

Fig. 1.9

Note that the experimental results in Figs. 1.5–1.8 represent fiberglass-reinforced plastics with polymer matrix. Related experimental studies were also conducted for other composites.

The paper [71] published in 1985 reports experimental results for a composite with an aluminum matrix reinforced with and compressed along unidirectional sapphire fibers. Figure 1.9 [71] shows a scaled-up image of fracture in the metal-matrix composite (sapphire fibers + aluminum) uniaxially compressed along unidirectional sapphire fibers. The fracture is localized in a relatively narrow zone. A plane drawn through the middle of the fracture zone in Fig. 1.9 is almost perpendicular to the line action of the compressive load.

Thus, when both fiberglass-reinforced plastics with polymer matrix (Figs. 1.6–1.8) and metal-matrix composites (Fig. 1.9) are compressed along reinforcement, fracture occurs or propagates almost transversely to the line of action of the compressive load, which is a specific feature of this type of fracture. However, fracture of this type does not occupy the entire volume of the material instantaneously though it begins with microbuckling in the composite. It is quite natural that this type of fracture may arise near any microinhomogeneity (discontinuity) and then proceed as describe above. In this connection, it is of interest to study the propagation of fractures near a macroinhomogeneity in a composite compressed along the fibers.

The paper [72] published in 1991 reports experimental results (Figs. 1.10–1.13) on the propagation of fractures from a circular hole in a composite plate compressed along the reinforcement.

Figure 1.12 shows a design model and the axes of coordinates (compression is along the vertical axis *Oy*). The plates are composite laminates, each ply being a unidirectional fibrous material (epoxy resin matrix reinforced with carbon fibers). The plies were laid up (along the *Oz*-axis in Fig. 1.12) so that the *Ox*- and *Oy*-axes (Fig. 1.12) were the axes of material symmetry (cross-ply laminate).

Hence, this composite can be approximated by an orthotropic material compressed along the *Oy*-axis, the *Ox*-, *Oy*- and *Oz*-axes (Fig. 1.12) being the axes of material symmetry. In the cross-ply laminates, the unidirectional fibers within most plies are aligned with the *Oy*-axis (Fig. 1.12). In this connection, the laminated plates can be considered to be mainly reinforced along the *Oy*-axis along which they are compressed.

In these experiments, fracture began at two points (indicated by "×" in Fig. 1.12) on the edge of the hole, i.e., the points at which the concentration of compressive macrostresses is maximum (stresses predicted by the orthotropic model). The fracture was further developed as two almost straight cracks filled with destroyed material, originated at points (indicated by "×" in Fig. 1.12) on the edge of the hole, and propagating almost transversely to the line of action of the compressive load. The behavior of cracks (fracture) is demonstrated by the electron microscope images in Figs. 1.10, 1.11, and 1.13 [72], where the scale in μm is indicated in the right lower corner. Figures 1.10, 1.11, and 1.13 show fracture propagating from the right point "×" in Fig. 1.12. For example, Fig. 1.10 shows a crack propagating from the hole almost transversely to the line of action of the compressive load. Figure 1.11 shows (at 20× magnification) the damaged portion of the material in an extending narrow band, which can be modeled by a filled crack. In Figs. 1.10 and 1.11, the compressive load is on the order of 95% of the ultimate load for the plate with a hole. Figure 1.13 shows the structure of the damaged portion of the material on the edge of the hole throughout the thickness (along the *Oz*-axis in Fig. 1.12) of the plate. The following types of fracture can clearly be seen: breaking of fibers, bending of broken fibers toward the hole, delamination of the laminated material. In Fig. 1.13, the compressive load is on the order of 80–85% of the ultimate load for the plate with a hole.

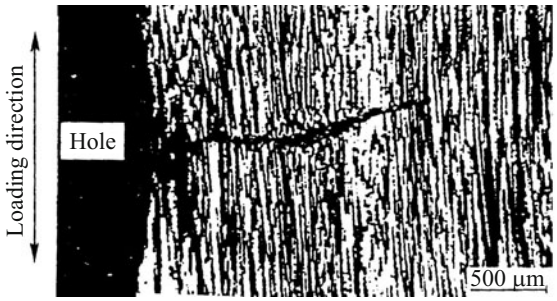

Fig. 1.10

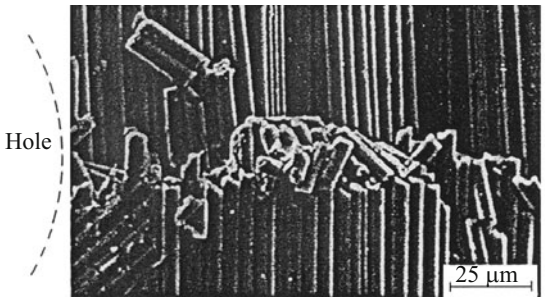

Fig. 1.11

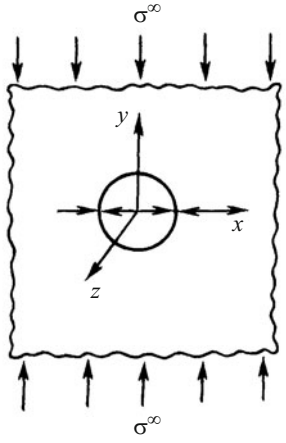

Fig. 1.12

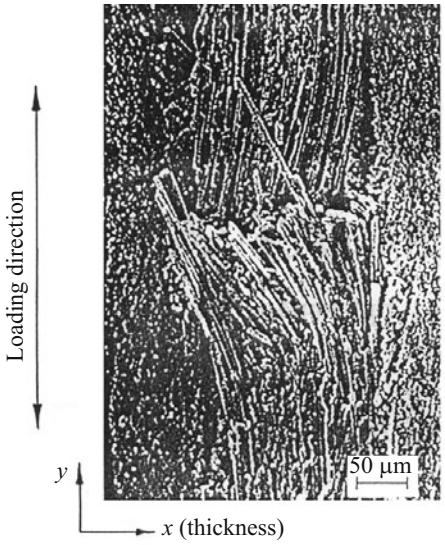

Fig. 1.13

It should be noted that in analyzing fracture in the internal structure of composites (as in Figs. 1.6–1.12 and 1.13), many authors mention only microbuckling and delamination. Actually, as can be seen from Fig. 1.11, there are much more failure mechanisms in the microstructure of a compressed composite such as breaking of a fiber within a crack, bending of a broken fiber, breaking of a fiber outside the crack, separation of a fiber from the matrix, fracture of the matrix, etc. These and similar failure mechanisms in the microstructure of a composite compressed along the axes of material symmetry manifest themselves only at subsequent stages of fracture, while the initial stage (start) of fracture is, apparently, microbuckling in the composite.

Fracture can, naturally, start near local inhomogeneities (such as cuts of fibers caused by the metal rings in Figs. 1.6–1.8) in the internal structure of the composite and near macroinhomogeneities (near the hole in Figs. 1.10–1.13). The local fracture in Figs. 1.5–1.13 then propagates along planes and surfaces that are almost perpendicular to the line of action of the compressive load. As repeatedly mentioned, this is a specific feature of the type of fracture under consideration.

The experimental results represented in Figs. 1.5–1.13 and related ones were published in 1968–1991. Such experimental studies are also conducted in the 21st century. Let us discuss, as an example, the experimental results published in [74] in 2004. These are results of experiments on a composite laminate consisting of 628 plies and subjected to compression along them. The number of plies is so great that we may assume that this material consists of an "infinite" number of plies. In this connection, the results in [74] may be considered to represent phenomena that occur in the internal structure of a composite laminate and do not depend on the boundary conditions for the whole laminate. It is, however, hardly possible to neglect the effect of boundary conditions, especially at the edges of the laminate, on all phenomena. Since the laminate was compressed along plies in [74], it may be assumed that the compression is along the axes of orthotropic symmetry (continuum approximation). Figure 1.14 [74, p. 1074, Fig. 2] shows the shapes taken by plies under compressive loads. The figure demonstrates narrow bands of destroyed material (shown by slanting solid lines in Fig. 1.14) that are periodic along the

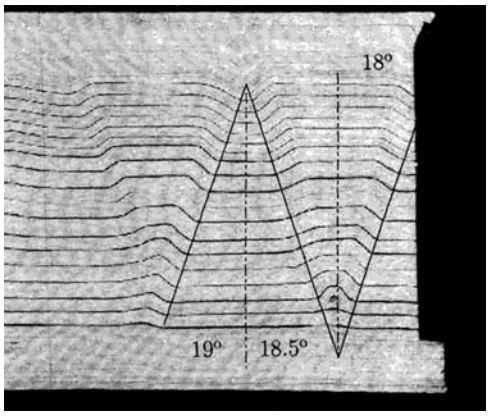

Fig. 1.14

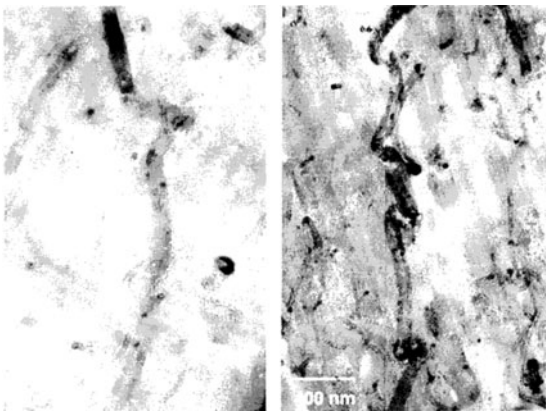

Fig. 1.15

horizontal axis. The experimental results represented in Fig. 1.14 will be discussed in the second part of the first section in analyzing so-called kinking, the term used in the English-language literature on the fracture mechanics of compressed composites.

1.1.3. Experimental Results for Nanocomposites under Compression. The active development of nanotechnologies in the last decades of the 20th century and in the beginning of the 21st century promoted the development of the mechanics of nanocomposites because the application of nanotubes in structural materials appeared to be clearly understood for nanocomposites only. Some idea of the development of nanocomposite mechanics can be gained from [12]. It should be noted that mainly polymer-matrix nanocomposites have currently been addressed. Due to the development of nanocomposite mechanics, the question has arisen of whether microbuckling can occur in nanocomposites, as in conventional composites (Sec. 1.1.1), which is also answered by conducting special experiments.

The buckling of a straight multiwall carbon nanotube (MWCNT) in a polymer matrix was observed in the paper [73] published in 2004. Figure 1.15 [73] shows multiple (multiwave) buckling of an MWCNT in a polymer matrix, the scale being indicated in the left lower corner of the figure. These buckling modes may be considered to be very complex and cannot be interpreted in a simple way. An examination of Fig. 1.15 does not reveal the separation of individual MWCNTs from the matrix. In this connection, we may conclude that the experimental results from [73] represented in Fig. 1.15 confirm the existence of the phenomenon of microbuckling in nanocomposites with polymer matrix. Note that this phenomenon was detected in [73] in pure form, as in Sec. 1.1.1 for conventional composites.

A somewhat different situation with the buckling of MWCNTs in a polymer matrix was observed in the experimental study [64] published in 1998. Note that in [64], as in Sec. 1.1.1, the composite was compressed due to the shrinkage of the polymer matrix. The results from [64] are represented by the TEM images in Figs. 1.16 and 1.17 for individual MWCNTs after shrinkage of the epoxy-resin matrix.

In these figures, the scale in nm is indicated in the upper left corner, and the shapes taken by individual MWCNTs after the shrinkage of the polymer matrix are schematized in the right lower corner. Figure 1.16 shows (in the left lower corner) a flexural buckling mode of an MWCNT, while Fig. 1.17 shows (in the right upper corner) a loop buckling mode of an MWCNT. In [64], these mode shapes are assumed to result from buckling and collapse. A close examination of Figs. 1.16 and 1.17 reveals that the nanotubes separate from the matrix where they bend and fold. This conclusion follows from the fact that the places where deformed parts of the nanotubes were earlier are shown as lighter background under each "bulge" (the left lower and right upper corners of Figs. 1.16 and 1.17).

Thus, the experimental results (Figs. 1.16 and 1.17) from [64] represent local fracture initiated by buckling. Hence, the experimental results from [64] represent the fracture of nanocomposites under compression (related results for conventional composites are discussed in Sec. 1.1.2). However, the experimental results from [64] do not confirm that the microbuckling phenomenon can occur in nanocomposites. Experimental results confirming that microbuckling can occur in conventional composites are discussed in Sec. 1.1.1. The above features of the experimental results from [64] were specified in [47] where it was pointed out that this situation had not been reflected in the subsequent reviews by the other authors. The results in Figs. 1.16 and 1.17 were also analyzed in [8].

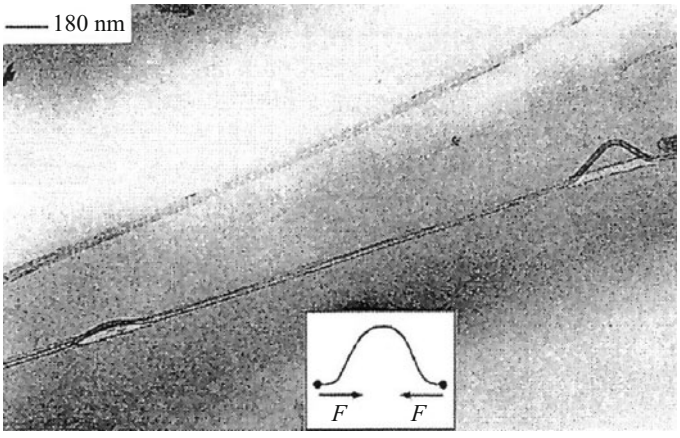

Fig. 1.16

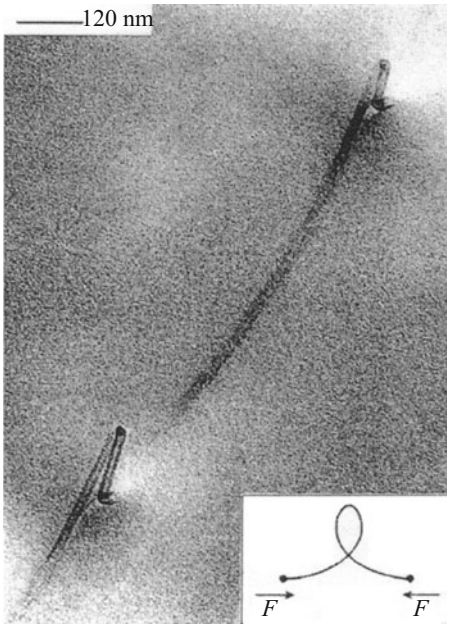

Fig. 1.17

In summary, the discussion of the experimental results from [64] should be supplemented with the following physical considerations on loop buckling shown in Fig. 1.17. Apparently, loop buckling cannot occur without fracture. This is because loop buckling of an MWCNT without fracture (separation of the nanotube from the matrix) would result in the ambiguity of displacements of the matrix.

1.1.4. General Characteristic of the Experimental Results. Here we will briefly characterize the areas and results of experimental studies on the microbuckling phenomenon that initiates failure or fracture of composites compressed along the axes of material symmetry.

The areas and results of experimental studies to be discussed may be divided into three groups.

First Group. The first group includes results that confirm the existence of the microbuckling phenomenon in composites compressed along the axes of material symmetry. To confirm that microbuckling can occur in its pure form (without fracture) in composites with various reinforcements (fibers), special experiments are usually conducted in which fibers are compressed due to the shrinkage of the polymer matrix. This type of loading was used in all studies of which we are aware. The experimental results discussed in Secs. 1.1.1 and 1.1.3 can be assigned to the first group. The above-mentioned results may be considered to confirm that the microbuckling phenomenon can occur in composites with various reinforcements, including nanocomposites, compressed along the reinforcement (fibers) for both infinite-fiber and finite-fiber models. Microbuckling in compressed composites is obviously the most likely fracture initiation mechanism similar to that in structural members (rods, plates, or shells) compressed along the axes of geometrical and material symmetry.

Second Group. This group includes experimental results on the fracture of composites compressed along the axes of symmetry and modeled by orthotropic materials, much attention being given to fracture behavior. The experimental results for composites with polymer or metal matrix discussed in Sec. 1.1.2 can be assigned to the second group. It should be noted that the results on fracture behavior shown in Figs. 1.5–1.13 are surely not exhaustive. Section 1.1.2 exemplifies experimental results of the second group of which we are aware. It follows from Figs. 1.5–1.11 and 1.13 that a typical feature of the fracture of composites modeled by orthotropic materials (continuum approximation) and compressed along the axes of material symmetry is the propagation of fracture within narrow bands that are almost perpendicular to the line of action of the compressive load. This is typical for composites with either polymer or metal matrix.

Third Group. This group includes experimental results on the fracture of composites modeled by orthotropic materials and compressed along the axes of material symmetry, including experimental values of ultimate strength and ultimate strain. It would be natural to compare the above experimental data with the theoretical results (theoretical ultimate strength and theoretical ultimate strain).

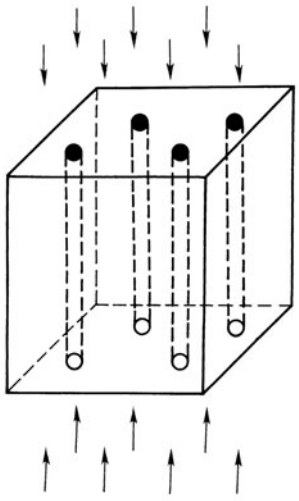

Fig. 1.18

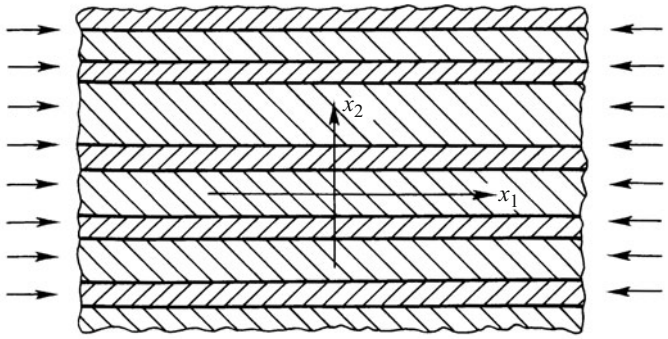

Fig. 1.19

Remark 1.3. There are quite many approaches to and theories for studying the microbuckling phenomenon in composites and, hence, analyzing the mechanism of fracture under compression. Quite approximate approaches and theories based on approximate and not always logical assumptions and hypotheses have become popular because making minor changes to these assumptions and hypotheses results in "new" approaches and theories, which is, in some cases, a pleasant situation for some authors. In this connection, we will not compare the experimental results with theoretical results obtained using such approximate approaches and theories, which seems to be what must be done in analyzing experimental results from the third group. In Sec. 1.2, however, experimental results on the fracture of composites compressed were compared with theoretical results using the most rigorous and consistent theory [7, 8] based on the TLTSDB [4–6, 43] (see [8] for more details).

In summary to Sec. 1.1 where experimental results in a certain field of the fracture mechanics of composites are analyzed, it should be pointed out that these results prove that microbuckling in composites is possible and demonstrate a specific feature in the fracture behavior of compressed composites for which microbuckling is the initial stage (start) of fracture. The above experimental results prove the relevance of the problems being considered and the necessity of theoretical studies involving the development of approaches, models, and methods and the obtaining of results for certain composites. Theoretical and experimental results are usually analyzed in reviews such as [45, 61, 62] published in the last two years.

1.2. Analysis of Theoretical Results. Here we will briefly discuss the basic concept defining the areas of theoretical studies. Also, we will briefly analyze theoretical results (approaches, models, methods, and specific results) for fibrous and laminated composites under compression obtained using the infinite-fiber model.

1.2.1. Formulation of the Basic Concept. The basic concept underlying the theoretical studies discussed below will be formulated based on the analysis of experimental results from Sec. 1.1.

Thus, we will consider composites modeled, in continuum approximation, by orthotropic materials and subjected to uniaxial, biaxial, or triaxial compression along the axes of material symmetry.

These materials include unidirectional fibrous composites compressed along the reinforcement (fibers) (Fig. 1.18). These materials also include composites reinforced with fibers laid in two perpendicular directions. Such a composite can be obtained by additionally reinforcing the material in Fig. 1.18 with unidirectional fibers along the horizontal axis.

These materials include laminated composites consisting of plies of dissimilar materials alternating along the Ox_2-axis (Fig. 1.19 where compression along the plies is shown). The plies of the composite laminate schematized in Fig. 1.19 can be made of different materials and these materials can be isotropic. Moreover, these laminated composites include cross-ply fiber-reinforced materials (Fig. 1.19). Note that the range of methods of producing laminated composites that can be modeled, in continuum approximation, by an orthotropic material can be extended considerably.

Figures 1.18 and 1.19 exemplify such composites.

Thus, the basic concept defining areas of theoretical studies can be formulated as follows.

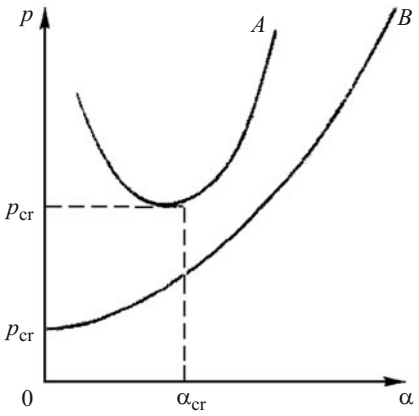

Fig. 1.20

Basic Concept. The initial stage (start) of fracture of composites modeled, in continuum approximation, by orthotropic materials and compressed along the axes of material symmetry is microbuckling. The propagation of fracture, which originates near macro- and microinhomogeneities, is determined by the behavior of perturbations in the theory of stability used (either relatively approximate or rather rigorous). The theoretical ultimate compressive strength and theoretical ultimate compressive strain are critical load and critical strain predicted by the theory of stability.

The basic concept in the fracture mechanics of compressed composites is similar to the situation in the mechanics of structural members (rods, plates and shells) where buckling is the initial stage of structural failure of structural members compressed along their axes of symmetry.

It makes sense to define the notion of microbuckling used in the basic concept. This notion can be rigorously and consistently formulated based on the piecewise-homogeneous model of a composite, following, for example, the monographs [8, Vol. 1, pp. 293–295]. In this case, by microbuckling is meant buckling in a composite that occurs at certain ratios between the stiffness characteristics and concentrations of the reinforcement and the matrix, which allowing determining the critical load and buckling mode irrespective of the type of structural member and the type of its boundary conditions.

We can now formulate the existence condition for the microbuckling phenomenon in a structural member made of a certain composite. Let us introduce the following notation: p_{cr} is the critical load causing microbuckling in the composite; p_{cr}^{sm} is the critical load causing buckling of the structural member; L is the typical (minimum) size of the structural member; l_{cr} is the microbuckling half-wavelength in the composite. With this notation, the microbuckling conditions are expressed as

$$p_{cr} < p_{cr}^{sm}, \quad l_{cr} << L. \tag{1.1}$$

Thus, if the compressive load is continuously increased, microbuckling in the composite of which the structural member is made of occurs if (i) the critical load causing microbuckling in the composite is lower than the critical load causing buckling of the structural member and (ii) the microbuckling wavelength in the composite is much shorter than the typical (minimum) size of the structural member.

To determine the microbuckling load and mode shapes, the second inequality in (1.1) is usually analyzed for a composite of specific structure and infinite size to obtain the relationship between the load parameter p and wave number α:

$$p = p(\alpha), \quad \alpha = \pi \frac{h}{l}, \tag{1.2}$$

where h is the typical geometrical parameter of the composite (h is the minimum thickness of plies in a composite laminate (Fig. 1.19)); $h \sim R$ is the fiber radius in a unidirectional fibrous composite (Fig. 1.18)); l is the microbuckling half-wavelength (along plies and fibers) in the composite.

We may now conclude that microbuckling in a composite cannot occur for arbitrary relationship (1.2). As an illustration, the curves A and B in Fig. 1.20 represent two types of relationship (1.2).

Since the curve A has a well-defined minimum, the value of p_{cr} can be found by minimizing the first expression in (1.2), and the expression $p_{cr} = p(\alpha_{cr})$ holds. Thus, if (1.1) is represented by the curve A in Fig. 1.20, we can determine the critical load p_{cr} and the buckling mode corresponding to the wave number $\alpha_{cr} = \pi h l_{cr}^{-1}$. Note that for the curve A, the following relations hold:

$$\alpha_{cr} \neq 0, \quad l_{cr} \neq \infty. \tag{1.3}$$

With (1.3) and (1.2) represented by the curve A in Fig. 1.20, conditions (1.1) are used for structural members in which microbuckling occurs in the composite they are made of.

The curve B in Fig. 1.20 is a monotonic curve; hence, by minimizing expression (1.2) we get the formula $p'_{cr} = p(0)$, and

$$\alpha_{cr} = 0, \quad l_{cr} = \infty. \tag{1.4}$$

From expressions (1.4) it follows that if (1.2) is represented by the curve B in Fig. 1.20, it is impossible to determine the microbuckling mode of the composite. Thus, if (1.2) is represented by the curve B in Fig. 1.20, then microbuckling does not occur in the composite. According to the second expression in (1.4), when (1.2) is represented by the curve B in Fig. 1.20, the second condition in (1.1) is satisfied for no structural member; hence, only the whole structural member can buckle.

Thus, microbuckling in the composite does not occur if the dependence of the load parameter p on the wave number α (the first expression in (1.2)) is represented by the curve B in Fig. 1.20. When (1.2) is represented by the curve A in Fig. 1.20 and α_{cr} is slightly different from zero, microbuckling in structural members does not occur too because of the second condition in (1.1) since $l_{cr} \to \infty$. This should be taken into account in analyzing this phenomenon in specific composites.

The basic concept outlined here (Sec. 1.2.1) and the approaches based on it will be used in Secs. 1.2.2–1.2.4 in analyzing the theoretical results on periodic (along reinforcement (fibers, plies) buckling modes obtained using the infinite-fiber model.

Currently, there are two approaches to studying the stability of composites and the fracture of composites under compression.

One approach is approximate and is based on various approximate design models and assumptions. The paper [16] published in Russian in 1967 is considered to be the first to use this approach. Later, this approach was further developed. Major publications on this approach are cited in [8].

The other approach, which is rigorous and consistent, is based on the three-dimensional linearized theory of stability of deformable bodies (TLTSDB) outlined in [4–6, 43]. This approach was for the first time proposed in the papers [2, 3, 30] published in 1969. Later, this approach was further developed. Major publications on this approach are cited in [8].

It should be noted that the second approach based on [2, 30] is the most rigorous, consistent, and accurate in solid mechanics.

1.2.2. Analysis of Theoretical Results. First (Approximate) Approach. Models and specific results obtained using the first approach are based on the basic concept outlined in Sec. 1.2.1.

1.2.2.1. Generalities. A typical feature of the first approach is the use of various approximate assumptions in studying microbuckling in composites, which is the initial stage (start) of fracture of composites under compression. A great many results on the mechanics of composites and fracture mechanics have been obtained using the first approach. In this connection, our goal here is not to review and analyze all such.

The objective of the present section (Sec. 1.2.2) is to classify results obtained with the first approach, to formulate the basic assumptions typical for the first approach, and to review the first publications on the first approach and the results they report.

The assumptions widely used by the first approach can be divided into four groups.

1. To analyze the stability of reinforcement (fibers, plies), wide use is made of applied one- and two-dimensional theories of stability of thin-walled systems (rods, plates) based on the Bernoulli hypotheses, Kirchhoff–Love hypotheses, etc. Such theories are known to be applicable only to the description of relatively long-wave buckling modes.

2. As a rule, the fact that the matrix (binder) also takes up a compressive load is ignored. This assumption can be made because the reinforcement is much stiffer than the matrix. Thus, the matrix can be considered unloaded.

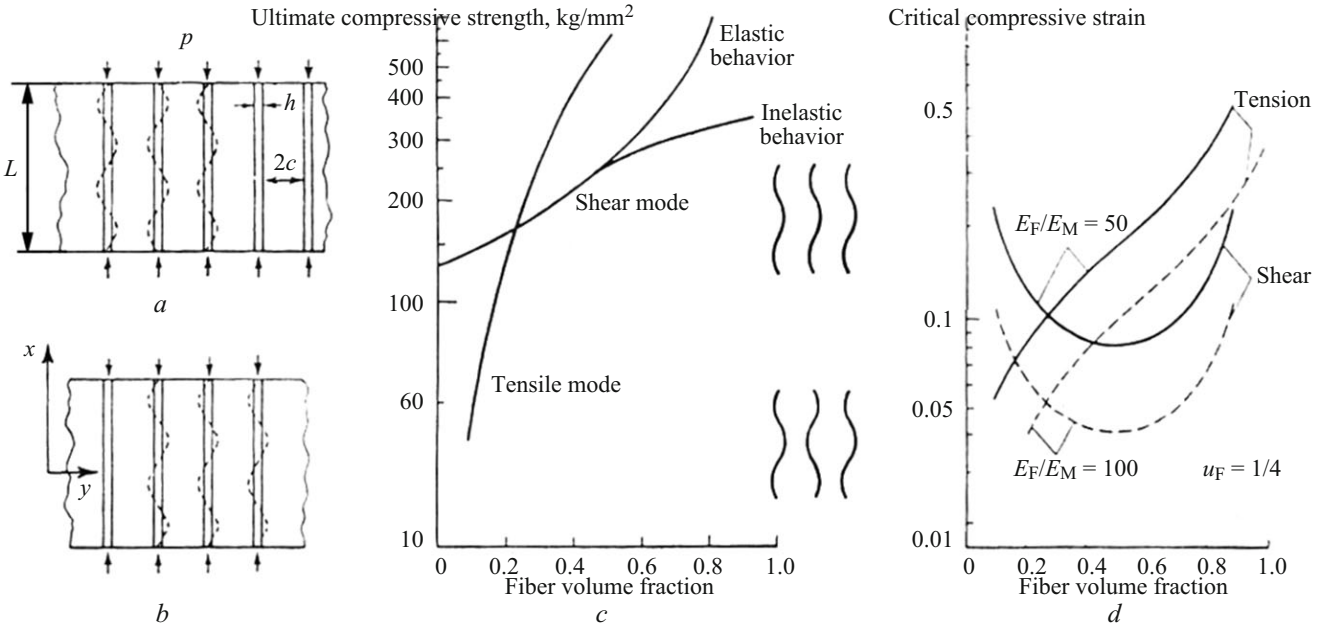

Analytical model of compressive strength of fibrous composite: tensile mode (*a*), shear mode (*b*)

Compressive strength of fiberglass-reinforced plastic

Critical compressive strain of fibrous composites

Fig. 1.21

3. The interaction between the matrix (binder) and the reinforcement (fibers, plies) is described approximately. To describe the interaction between the matrix and a fiber, the matrix is frequently modeled by a coaxial cylinder (a part of the matrix). A one-dimensional model of the matrix can be used as well.

4. The interface conditions between the reinforcement and the matrix are satisfied approximately, frequently without any explanation.

If one of these assumptions is made, other assumptions are introduced automatically. To illustrate this situation, we will consider the following example. For example, if it is assumed that compression of a composite does not affect the matrix and induces stresses in the reinforcement (second group of assumptions), then it is also assumed that the interface conditions between the matrix and the reinforcement (fourth group of assumptions) are satisfied approximately. The matter is that the initial assumption automatically means that the matrix and reinforcement can freely slip relative to each other along the fibers in the subcritical state (before buckling) and are perfectly bonded during buckling. Certainly, the assumptions of the four groups and other assumptions used by the first approach can be further analyzed, but such an analysis is not intended here. Moreover, in Sec. 1.2.3, we will analyze the second approach that does not use the above assumptions.

1.2.2.2. Analysis of the First Publication [26, 67]. As an example, we will analyze the results obtained using the first approach in [26], which is the first study based on this approach. It was published in Russian in 1967 and is the translation of the paper [67] published in 1965. Figure 1.21 presents the basic results from [26, Figs. 3.22–3.24]. It should be noted that all results in [26] were obtained on the assumption of plane strain in the plane *xy* in Fig. 1.21 (Fig. 3.22 in [26]), i.e., all results from [26] represent, strictly speaking, a composite laminate with plies infinite along the *Oz*-axis (perpendicular to the plane of Fig. 1.21). Hence, in [26] a unidirectional fibrous material is modeled by a plane that passes along the fibers (plane problem). Thus, the basic assumption in [26] can be formulated as follows.

Basic Assumption [26]. Microbuckling in a unidirectional fibrous composite can be studied by formulating a plane problem for a composite laminate.

Thus, a unidirectional fibrous composite was modeled by a composite laminate in [26], but the basic assumption was not formulated and no comments were made. In what follows, we will briefly discuss the basic results from [26] for a composite laminate, using the standard terminology and making no mention of the modeling.

In [26], specific results were obtained for the following periodic (along the *Ox*-axis) buckling modes using the infinite-fiber model: (i) tension mode (neighboring plies of the reinforcement buckle in antiphase; Fig. 1.21, [26, Fig. 3.22*a*]);

(ii) shear mode (all plies of the reinforcement and matrix buckle in the same flexural mode; Fig. 1.21, [26, Fig. 3.22*b*]). Also following assumptions are made in [26]:

– the reinforcement is described using an applied one-dimensional theory of stability of thin rods based on the Bernoulli hypotheses;

– the matrix does not take up a compressive load (in Fig. 1.21, only the reinforcement is loaded, and the load is indicated by arrows);

– the interaction between the matrix and the reinforcement is described using a one-dimensional model of the matrix;

– the interface conditions between the reinforcement and the matrix are approximately satisfied in the same sense as in the fourth group of assumptions.

Figure 1.21 shows the dependence of the theoretical ultimate compressive strength [26, Fig. 3.23] and the theoretical ultimate compressive strain in % [26, Fig. 3.24] on the volume fraction (concentration) ν_F of fibers in the composite.

The results from [26, 67] are well-known and generally recognized in the world's scientific literature on the mechanics of composites and fracture mechanics. For example, these results were included in the first part of the first volume of the seven-volume treatise on fracture [25]. Moreover, these results were included in the eight-volume treatise on composites [19] (the paper [20] on metal-matrix composites in the first volume and the paper [28] on materials with metal and polymer matrices in the fifth volume).

It should be noted that numerous studies based on the first approach are referred in [7, 8, 20, 27, 28]. Among such publications, the first ones were [70] published in English in 1966 and [68] published in English in 1967.

Thus, the theoretical studies [26, 67] and their quantitative results obtained using the first approach and being, apparently, the first in this field are universally recognized and included in all well-known reviews. What has been briefly outlined above (Sec. 1.2.2.2) is called the Dow–Gruntfest–Rosen–Schuerch theory (the names of the authors of [39, 67, 70]); this terms was used, for example, in [29] with reference to [27].

1.2.2.3. Comparative Analysis (*Validation*) *of the Results from* [26, 67]. Despite the popularity and recognition of the Dow–Gruntfest–Rosen–Schuerch theory and the corresponding quantitative results presented in Fig. 1.21, it should be pointed out that this theory and results are based rather approximate assumptions formulated in Sec. 1.2.2.1 for the first approach (as termed in the final part of Sec. 1.2.1 and in the monographs [7, 8] and concretized in Sec. 1.2.2.2 for [26, 67]). Note that the approximate assumptions discussed above were made in [26, 67] in setting up design models. In this connection, to validate the results (Fig. 1.21) from [26, 67], it is necessary to compare them with results obtained using more rigorous and well-founded assumptions.

As repeatedly mentioned, the second approach (as termed in the final part of Sec. 1.2.1 and in the monographs [7, 8]) based on the TLTSDB [6, 43] is the most rigorous, consistent, and accurate in solid mechanics. It is natural that the second approach does not use approximate assumptions typical for the first approach. Thus, to validate the results (Fig. 1.21) from [26, 67], it is expedient to compare them with results obtained using the second approach.

The results of the Dow–Gruntfest–Rosen–Schuerch theory (Fig. 1.21; [26, 67]) obtained using the first approach and the results obtained using the second approach were compared in [7, pp. 206–214] and then this comparative analysis was partially reproduced in [8, Vol. 1, pp. 187–189]. Note that different notation for the same parameters was used in [26] and in [7, 8]: Young's modulus, shear modulus, and volume fractions of the reinforcement and matrix were denoted, respectively, by E_F and E_M, G_F and G_M, ν_F and ν_M in [26] and by E_r and E_m, G_r and G_m, S_r and S_m in [7, 8]. Thus, the correspondence between the notation is as follows:

$$E_F \sim E_r, \quad E_M \sim E_m,$$
$$G_F \sim G_r, \quad G_M \sim G_m,$$
$$\nu_F \sim S_r, \quad \nu_M \sim S_m. \tag{1.5}$$

In view of (1.5), all details on the comparative analysis can be found in [7, 8].

We will now briefly discuss the qualitative contradictions and quantitative differences between the results (Fig. 1.21) of the Dow–Gruntfest–Rosen–Schuerch theory obtained using the first approach and the results [7, 8] obtained using the second approach, which does not use approximate assumptions typical for the first approach.

Qualitative Contradictions. We will restrict ourselves to two.

1. The theory [26, 67] does not permit the occurrence of microbuckling in shear mode for any composite (for any ratios between material and geometrical characteristics). This conclusion follows (according to the approaches outlined near Fig. 1.20) from the expression [6, p. 96; B. 26], which suggests that the function $p = p(\alpha)$ (1.2) is monotonic, as the curve *B* in Fig. 1.20. This conclusion was formulated in more detail in [7, pp. 207–209].

The second approach allows proving that microbuckling in shear mode can occur depending on the ratio between the material and geometrical characteristics of the composite. In particular, this shear buckling occurs when the concentration of reinforcement is low, which is noted in [7, p. 209].

Thus, we have formulated the first qualitative contradiction of the theory [26, 67].

2. When the concentration of reinforcement is high, the theory [26, 67] leads to physically an incorrect result for the shear mode. For example, from [26, p. 82, (3.29)] it follows that the theoretical ultimate compressive strength $\to \infty$ as $v_{\rm F} \to 1$or, which is equivalent, $v_{\rm m} \to 0$.

The second approach allows proving that the theoretical ultimate compressive strength tends to a finite value [8, Vol. 1, pp. 189, 271–295].

Thus, we have formulated the second qualitative contradiction of the theory [26, 67].

Quantitative Differences. We will restrict ourselves to two.

1. The results of the theory [26, 67] and the results of the second approach differ considerably at low and high concentrations (volume fractions) of the reinforcement (filler, fibers). This conclusion was formulated in [7, p. 210].

2. The results of the theory [26, 67] and the results of the second approach can differ by a factor of three and more at low concentrations of the reinforcement. This conclusion was formulated in [7, p. 211].

This is the quantitative error of the theory [26, 67].

Conclusions. We can now formulate the following conclusions on the Dow–Gruntfest–Rosen–Schuerch theory and its results [26, 67].

1. This theory and its quantitative results [26, 67] have significant qualitative contradictions and quantitative errors compared to the theory and the results obtained with accuracy typical for solid mechanics (the second approach, as termed in [7, 8] and in the final part of Sec. 1.2.1).

2. Conclusion 1 does not allow considering the Dow–Gruntfest–Rosen–Schuerch theory and its quantitative results [16, 41] reliable.

3. To validate specific results obtained using the Dow–Gruntfest–Rosen–Schuerch theory, it is necessary to conduct additional studies.

4. Conclusions 1–3 equally apply to other theories and results obtained with the first approach because it is based on approximate assumptions 1–4 (Sec. 1.2.2.1), which are the approximate assumptions of the Dow–Gruntfest–Rosen–Schuerch theory (Sec. 1.2.2.2).

Remark 1.4. Certainly, the Dow–Gruntfest–Rosen–Schuerch theory and its quantitative results [26, Figs. 3.23 and 3.24], as well as other theories and their results obtained with the first approach, could be validated by comparing with experimental data. We believe, however, that the above approach is difficult to implement and is not rational because of the following: (i) it is very difficult to conduct a special experiment representing, for example, the situation in [26, Fig. 3.22] and (ii) in developing theories using the first approach (such as the theory [26, 67]), numerous approximate theoretical assumptions are made to set up design models. In this connection, the priority task is to validate these approximate theoretical assumptions for theories constructed with accuracy typical for solid mechanics.

1.2.3. Analysis of Theoretical Results. Second (Rigorous and Consistent) Approach. Models and specific results obtained using the second approach are based on the basic concept outlined in Sec. 1.2.1. Unlike the first approach (Sec. 1.2.2), the second approach does not use various approximate assumptions briefly described in Sec. 1.2.2.1.

1.2.3.1. General Description. A typical feature of the second approach is the use of the TLTSDB [4–6, 43] to study microbuckling as the initial stage (start) of fracture of composites under compression. In this case, the theory of large (finite) subcritical deformations and the first and second theories of small subcritical deformations [6, 43] are used. The basic results corresponding to the second approach were reported in [4, 5, 7, 8] where [5] is devoted solely to the theory of large (finite) subcritical deformations.

As repeatedly mentioned, the second approach was for the first time proposed in the papers [2, 3, 30] published in 1969. The results that had been obtained with the second approach before 2008 are reported in the two-volume monograph [8] where the list of references includes main publications on the second approach. The second approach was used to develop the

continuum theory of the fracture of composites based on a homogeneous material model with effective characteristics and the three-dimensional theory of stability of fibrous and laminated composites under compression based on a piecewise-homogeneous material model with exact interface conditions. The second approach based on the piecewise-homogeneous material model first addressed in [2, 30] is the most rigorous, consistent, and accurate in solid mechanics. In this connection, results obtained with the second approach can be used to validate results obtained with the first approach, which was done, as an example, in Sec. 1.2.2.3.

It should be noted that internal fracture can be studied using either the second or the first approach. Moreover, the second approach can be used (in addition to the first approach) to study near-surface fracture initiated by near-surface microbuckling under compression along the reinforcements and end crushing initiated by near-surface microbuckling near the loaded ends.

The second approach was also used to study the behavior of elastic and elastoplastic, compressible and incompressible, isotropic, transversely isotropic, and orthotropic materials under compression along the axes of material symmetry. General results were obtained using elastic models for hyperelastic materials with arbitrary elastic potential and using elastoplastic models for materials with general constitutive equations. Specific results were obtained using elastic and elastoplastic models for materials with elementary constitutive equations.

For elastoplastic models (of matrix and reinforcement), use is made of the generalized concept of increasing load outlined in, for example, the monographs [6, 43]. In this connection, buckling problems are formulated in a general form for elastic and elastoplastic models.

The second approach is used to study microbuckling in composites under an external "dead" load, which is typical for all publications on fracture mechanics. For the second approach based on elastic and elastoplastic models (including the generalized concept of increasing load), it was strictly proved that the sufficient conditions for the applicability of the static method of stability analysis [6, 43] are satisfied; therefore, the buckling problems are reduced to eigenvalue problems, i.e., the Euler method is used. This proof is also valid in the cases of near-surface instability under compression along reinforcements and near-surface instability near loaded ends. Thus, using the second approach is fully consistent with the standard and rigorous method of studying buckling by analyzing the behavior of small perturbations in linearized three-dimensional dynamics.

Results of the second approach are intended for composites with polymer and metal matrix. For polymer-matrix composites, brittle fracture is analyzed by modeling the matrix by an elastic body, which is typical for composites at moderate temperatures and under relatively short-term load because the viscosity effects can be neglected in this case. For metal-matrix composites, ductile fracture is analyzed (using the generalized concept of increasing load) considering the stage of loading in which the entire matrix deforms plastically.

Remark 1.5. When the second approach is used to study microbuckling and near-surface buckling in a composite, it is assumed that the reinforcement and the matrix deform by equal amount along the line of compression (along the fibers in Fig. 1.18 for an unidirectional fibrous composite and along the plies (along the Ox_1-axis) in Fig. 1.19 for a laminated composite). The above is, apparently, the only condition that allows analyzing phenomena inside a composite. In experiments, such conditions are provided by compressing the composite with quite hard disks along the horizontal axis in Fig. 1.19 with minimum friction along the vertical axis in Fig. 1.19. In theoretical studies, the displacements of the reinforcement and the matrix along the Ox_1-axis are assumed equal, and the shear stresses along the Ox_2-axis are assumed zero.

This completes the rather brief description of the second approach in the mechanics of the fracture of composites compressed along the axes of material symmetry and modeled by an orthotropic material (continuum approximation). Such an approach is used to study microbuckling in a composite as the beginning (start) of the internal fracture of the whole and to study near-surface instability of a composite (compressed along the reinforcement, including compression at the ends) as the beginning (start) of the near-surface fracture of the composite.

We will now briefly discuss the developed methods and the results obtained using the homogeneous material model with effective characteristics (continuum theory) and the piecewise-homogeneous material model (most accurate formulation).

1.2.3.2. Continuum Fracture Theory. Let us briefly discuss the continuum theory of the fracture of compressed composites based on a continuum model with effective characteristics. The basic results were obtained for brittle and ductile fracture. In the latter case, the generalized concept of increasing load outlined in, for example, the monographs [6, 43] was used. In line with the basic approach outlined in Sec. 1.2.3.1, it is necessary to analyze the static equations and boundary conditions of the TLTSDB [6, 43]. The major results were obtained for microbuckling (internal fracture) and for near-surface buckling (near-surface fracture) (see [8, Vol. 1, Ch. 2] for more details).

1.2.3.2.1. Internal Fracture. Internal fracture should be studied for an unbounded composite. The propagation of fracture is described by a system of static TLTSDB equations [6, 43], which is elliptic for a compressible material under no load. In continuum approximation, the compressibility of a composite is due to the compressibility of either the reinforcement or the matrix.

Since the material under consideration is unbounded, internal fracture is considered as buckling of a microvolume. Thus, changes in a microvolume must be somehow manifested in a macrovolume, and they must not be local because only in this case, fracture of the whole specimen (macrofracture) will be observed. Such changes in a microvolume must manifest themselves in the properties that are independent of the boundary conditions because it is the fracture of the material (internal fracture corresponds to an "infinite" material) that is studied rather than the influence of the testing machines, the shape of the cross section, etc. It is obvious that changes in a macrovolume are determined by perturbed displacements that are described by the system of static TLTSDB equations [6, 43].

Thus, fracture may be considered to start when the solutions (except for homogeneous stress–strain states) of the system of static TLTSDB equations [6, 43] for a compressible material become independent of the boundary conditions (the material is unbounded) and nonlocal. This condition for the system of static TLTSDB equations [6, 43] can be satisfied only when this system is hyperbolic.

Considering the foregoing, we can formulate the basic concept underlying the continuum theory of internal fracture of compressed composites as follows.

The fracture onset can be identified with that instant in the history of loading when the system of static TLTSDB equations (for compressible materials) changes over from elliptic into hyperbolic, i.e., the system loses the property of ellipticity. The theoretical ultimate strength is determined from the same condition. The fracture of compressed composites occurs along characteristic planes and surfaces.

More details can be found in [8, Vol. 1, Ch. 2]. We will consider only some results.

Following the basic concept, we introduce the concept of surface Π_{T} of theoretical ultimate compressive strengths in the three-dimensional space of principal compressive stresses. In the case of brittle fracture (polymer-matrix composites), the surface Π_{T} was constructed explicitly for three- and two-dimensional problems. Also, it was strictly proved that brittle fracture propagates along planes perpendicular to the line of action of compressive loads. This theoretical fact is in agreement with the experimental results in Figs. 1.5–1.8 and 1.10.

We will now compare, following [8, Vol. 1, Ch. 2], the theoretical ultimate compressive strengths and theoretical ultimate compressive strains calculated with the continuum theory of internal fracture (Sec. 1.2.3.2.1) and found experimentally. According to the classification of Sec. 1.1.4, these experimental studies fall into the third group.

Brittle Fracture. Let us consider a unidirectional fibrous composite with epoxy resin matrix and quite stiff fibers, for which

$$E_{\mathrm{r}} >> E_{\mathrm{m}}. \tag{1.6}$$

We introduce the following notation: $(\Pi_3^-)_{\mathrm{T}}$ is the theoretical ultimate strength in compression along one axis (in our case, the Ox_3-axis); $(\Pi_3^-)_{\mathrm{ex}}$ is the experimental ultimate strength in compression along the same axis. In the case of (1.6), the theoretical ultimate compressive strength (found using the continuum theory of fracture) for a composite with 50% volume fraction of unidirectional fibers ($S_{\mathrm{r}} = S_{\mathrm{m}} = 0.5$) was given in [8, Vol. 1, p. 192]:

$$(\Pi_3^-)_{\mathrm{T}} = 2.09\text{–}3.00 \text{ GPa} \tag{1.7}$$

taking into account the spread in the properties of the epoxy resin specified in [8, Vol. 1, Table 0.1, p. 67)]. The handbook [24] published in Russian in 1981 (and translated into English in [59] in 1978) gives (on p. 656) experimental ultimate strengths for various composites (different fibers for $S_{\mathrm{r}} = S_{\mathrm{m}}$). These results were also presented in [8, Vol. 1, p. 192] in the form

$$(\Pi_3^-)_{\mathrm{ex}} = \begin{cases} 3.10\,\text{GPa for boron fibers,} \\ 1.38\,\text{GPa for high-strength carbon fibers,} \\ 1.03\,\text{GPa for high-modulus carbon fibers.} \end{cases} \tag{1.8}$$

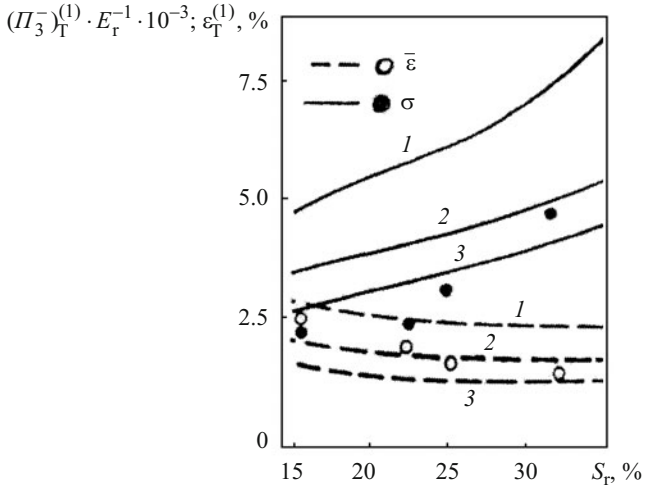

Fig. 1.22

Comparing (1.7) and (1.8), we see that polymer-matrix composites quite good correspondence between theoretical ultimate strengths on compression and experimental ultimate strengths is observed at uniaxial compression.

Ductile Fracture. Let us consider a unidirectional fibrous material with pure aluminum matrix and stainless-steel wire reinforcement. Experimental results for this composite are reported in [66]. The theoretical ultimate strength and theoretical ultimate compressive strain (calculated using the continuum theory of internal fracture) were determined in the first approximation in the monograph [8, Vol. 1, Ch. 2, pp. 193–202] where the reinforcement was modeled by a linear elastic isotropic compressible body and the matrix was modeled by an elastoplastic isotropic incompressible body with power relationship between intensities of stresses and strains:

$$\sigma_u^m = A_m \varepsilon_u^{mk_m}, \quad A_m \text{ and } k_m \text{ are constants.} \tag{1.9}$$

In [66], the experimental results were given for different concentrations in % of the reinforcement (S_r = 4.1, 11, 15.3, 21.2, 24.8, 32.8). To save space, Fig. 1.22 shows (in contrast to [8, Vol. 1, Ch. 2, Fig. 2.9, p. 206)] results only for the following values of S_r (%): 15.3, 21.2, 24.8, 32.8. In [8, Vol. 1, Ch. 2, Fig. 2.9, p. 206], the factor E_r^{-1} (E_r is Young's modulus of the reinforcement (stainless steel wire) according to (1.5)) was left out. This is corrected in Fig. 1.22.

In describing the plastic deformation of pure aluminum using formula (1.9), the following three approximations for A_m and k_m in (1.9) were used:

$$\begin{aligned} 1 &\sim A_m = 100\,\text{MPa}, \quad k_m = 0.1, \\ 2 &\sim A_m = 100\,\text{MPa}, \quad k_m = 0.25, \\ 3 &\sim A_m = 68\,\text{MPa}, \quad k_m = 0.25. \end{aligned} \tag{1.10}$$

The monograph [8, Vol. 1, Ch. 2, p. 207] cites publications that used approximations (1.10).

Figure 1.22 shows the dependence of the following quantities on S_r (volume fraction of stainless steel wire): dimensionless normalized theoretical ultimate compressive strength $(\Pi_3^-)_T^{(1)} \cdot E_r^{-1} \cdot 10^{-3}$ calculated in the first approximation (solid lines) and theoretical ultimate strain $\varepsilon_T^{(1)}$ calculated in % in the first approximation (dashed lines).

The curves in Fig. 1.22 corresponding to approximations (1.10) are numbered by *1*, *2*, and *3*. The experimental results from [50] are shown in Fig. 1.22 by full circles for the ultimate strength and by open circles for the ultimate strain. Note that approximation 2 was used in [50].

Figure 1.22 indicates that the satisfactory agreement between the theoretical and experimental results is observed for ultimate strengths when approximation 3 in (1.10) is used and for ultimate strains when approximation 2 in (1.10) is used.

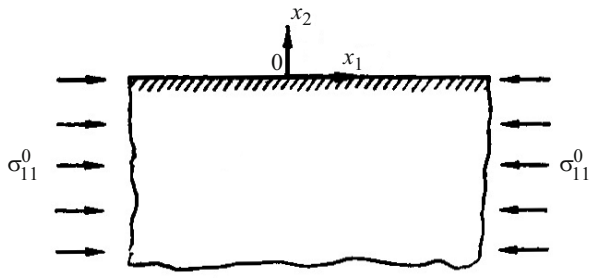

Fig. 1.23

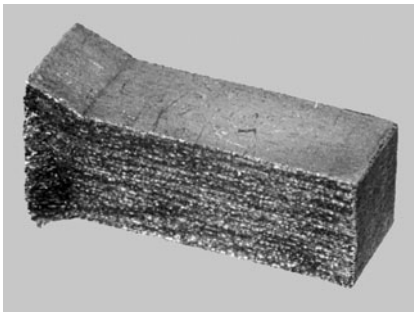

Fig. 1.24

This completes the discussion of the mechanics of internal fracture within the framework of the continuum theory of fracture (see [8, Vol. 1, Ch. 2] for more details).

1.2.3.2.2. Near-Surface Fracture. The continuum theory of near-surface fracture is based on the TLTSDB [6, 30] used to study a near-surface buckling mode within which displacements and stresses decay with distance from the boundary. Following the basic approach outlined in Sec. 1.2.3.1, we arrive at static TLTSDB problems [6, 30] for semibounded domains (eigenvalue problems in which eigenfunctions decay with distance from the boundary).

As already mentioned in Sec. 1.2.3.1, the continuum theory of near-surface fracture addressed two types of such fracture: (i) near-surface fracture due to near-surface buckling in compression along reinforcement and (ii) end crushing due to near-surface buckling near the loaded ends.

The continuum theory of near-surface fracture of type (i) is detailed in [8, Vol. 1, Ch. 2, Sec. 2, pp. 209–224)]. As an example, Fig. 1.23 shows a design model for a plane problem for type (i) of fracture, where $x_2 = 0$ is the free surface and the reinforcement is aligned with the Ox_1-axis.

The continuum theory of near-surface fracture of type (ii) is detailed in [7, Ch. 7, Sec. 4, pp. 568–589)]. As an example, Fig. 1.24 [8, Vol. 1, Ch. 4, p. 486, Fig. 4.30] presents results of experimental observation of end crushing for specimens made of unidirectional boron aluminum composite (these results were published in [13]).

Thus, the monographs [7, 8] detail the continuum theory of near-surface fracture due to near-surface buckling in compression along the reinforcement and the continuum theory of near-surface fracture due to near-surface buckling near the loaded ends (end crushing). Results were presented for polymer-matrix composites (brittle fracture) and for metal-matrix composites (ductile fracture). The monograph [8, Vol. 1, Ch. 2, Sec. 2] also outlines the two-level continuum mesomechanics of fracture of compressed composites with cracks near holes.

In summary, it should be pointed out that in [7, 8], the following conditions were strictly proved for composites with polymer and metal matrices:

$$(\Pi_3^-)_{\mathrm{T}}^{\mathrm{EC}} < (\Pi_3^-)_{\mathrm{T}}, \quad (\Pi_3^-)_{\mathrm{T}}^{(\mathrm{i})} < (\Pi_3^-)_{\mathrm{T}}, \tag{1.11}$$

where the following notation is introduced in addition to $(\Pi_3^-)_{\mathrm{T}}$ (theoretical ultimate strength in uniaxial compression): $(\Pi_3^-)_{\mathrm{T}}^{(\mathrm{i})}$ is the theoretical ultimate strength in uniaxial compression for fracture of type (i); $(\Pi_3^-)_{\mathrm{T}}^{\mathrm{EC}}$ is the theoretical ultimate strength in uniaxial compression for fracture of type (ii) (end crushing). Conditions (1.11) are consistent with the commonly accepted fact that fracture begins on the surface of a material.

Remark 1.6. In Sec. 1.2.3.2.1, it is shown that the experimental and theoretical ultimate strengths in uniaxial compression are in agreement for both brittle fracture (polymer-matrix composites) and ductile fracture (metal-matrix composites). This agreement is apparently due to the fact that the reinforcement and matrix of the composites analyzed were considered differ considerably in stiffness (conditions (1.6) are satisfied). For other composites, such good agreement is hardly achievable. It should be pointed out that the continuum theory of fracture is the most simple and convenient compared with any theories based on the piecewise-homogeneous material model for approaches. In some cases, the continuum theory appears in agreement with experiments. Historically, the paper [3] published in 1969 was the first to address the continuum theory of fracture.

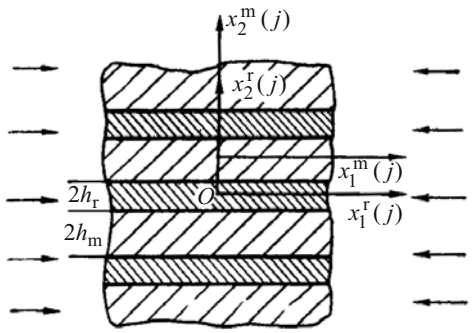

Fig. 1.25

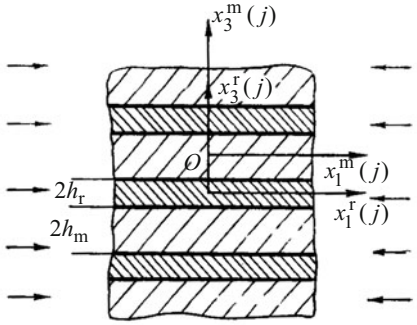

Fig. 1.26

1.2.3.3. Laminated Composite. Piecewise-Homogeneous Material. Here we will briefly discuss the mechanics of fracture of compressed composite laminates with polymer and metal matrices based on the piecewise-homogeneous material model. The TLTSDB [6, 43] is applied to each ply of the reinforcement and matrix, and continuity conditions for stresses and displacements are prescribed at the interfaces. The basic results were obtained for brittle and ductile fracture. In the latter case, the generalized concept of increasing load outlined in, for example, the monographs [6, 43] was used. In line with the basic approach outlined in Sec. 1.2.3.1, it is necessary to analyze the static equations and boundary conditions of the TLTSDB [6, 43] for a piecewise-homogeneous material (eigenvalue problem). The basic results were obtained for microbuckling [8, Vol. 1, Ch. 3] and for near-surface buckling [8, Vol. 1, Ch. 5]. The list of references in [8] includes publications on stability of composite laminates analyzed using the second approach (as termed in Secs. 1.2.1 and 1.2.3.1 and in the monographs [7, 8]).

1.2.3.3.1. Internal Fracture. The internal instability of an unbounded composite laminate (Fig. 1.19) is analyzed using the general solutions of the static TLTSDB equations [6, 43] and the procedure outlined in Sec. 1.2.1, taking into account the approach corresponding to Fig. 1.20. It should be noted that here we discuss results for composites with no defects at the interfaces (continuity of stresses and displacements at the interfaces). Results for composites with interfacial defects are discussed in Sec. 1.2.3.3.3.

Two- and three-dimensional problems were solved for laminated composites with polymer and metal matrices consisting of reinforcement plies (of equal thickness) and matrix plies (of equal thickness) that periodically alternate along the Ox_2-axis (Fig. 1.25) in the case of plane problems and along the Ox_3-axis (Fig. 1.26 corresponding to the plane $x_2 = 0$) in the case of spatial problems. In Figs. 1.25 and 1.26, as in (1.5), the index "r" refers to reinforcement (filler, plies) and the index "m" refers to the matrix (binder, plies). The plies are made of orthotropic materials (or isotropic materials in a special case) in the plane case and of transversely isotropic materials (or isotropic materials in a special case) with the isotropy plane $x_3 = \text{const}$ (Fig. 1.26). In all cases, the characteristic determinants were obtained for materials described by general constitutive equations. Since the structure is periodic with period $2(h_{\mathrm{r}} + h_{\mathrm{m}})$ along the vertical axis in Figs. 1.25 and 1.26, buckling modes with period T_k multiple of the period of the structure were analyzed,

$$T_k = 2k(h_{\mathrm{r}} + h_{\mathrm{m}}), \quad k = 1, 2, \ldots . \tag{1.12}$$

The first four modes called modes of the first, second, third, and fourth kinds (schematized in Figs. 1.27–1.30) were analyzed. The buckling mode of the first kind has a period equal to the period of the structure ($k = 1$ in (1.12)) and is shown in Fig. 1.27; in Fig. 1.21 (Fig. 3.22) this mode corresponds to the shear mode.

The buckling mode of the second kind has a period equal to the double period of the structure ($k = 2$ in (1.12)) and is shown in Fig. 1.28; in Fig. 1.21 (Fig. 3.22) this mode corresponds to the tension mode.

The buckling mode of the third kind has a period equal to the period of the structure ($k = 1$ in (1.12)) and is shown in Fig. 1.29.

The buckling mode of the fourth kind has a period equal to the double period of the structure ($k = 2$ in (1.12)) and is shown in Fig. 1.30.

In the plane and spatial cases, characteristic determinants were derived in closed form for the reinforcement and polymer and metal matrices of laminated composites described by general constitutive equations. The critical loads were

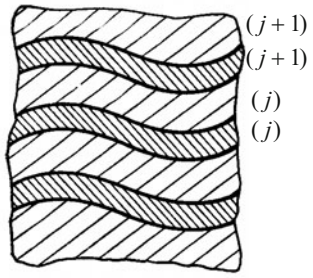

Fig. 1.27

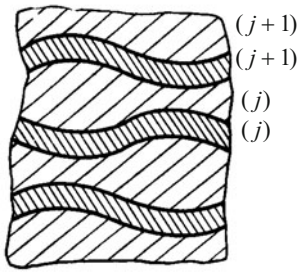

Fig. 1.28

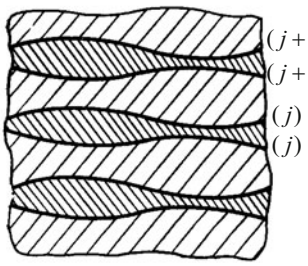

Fig. 1.29

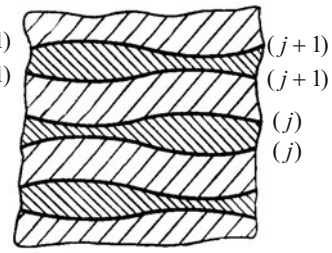

Fig. 1.30

obtained by finding numerically and minimizing the roots of the characteristic determinants. This approach helped to obtain numerous results for specific laminated composites with either polymer or metal matrix.

As an example, we will briefly discuss results for a composite laminate with isotropic plies, each modeled by a linear elastic body. These results were detailed in [8, Vol. 1, pp. 297–299]. Figure 1.31 (replicating Fig. 3.9 from [8]) shows the dependence of the load parameter on the wave number α_r (as in (1.2)) for a composite laminate with the following parameters in the plane case: $E_r \cdot E_m^{-1} = 500$; $h_m \cdot h_r^{-1} = 1$, 5, 10, 20, 30, 40, 50 (curves *1–7*, respectively), the notation corresponding to Fig. 1.25. The solid lines represent the bending mode (buckling mode of the first kind, Fig. 1.27), while the dash-dot lines represent the tension mode (buckling mode of the second kind, Fig. 1.28).

Let us briefly analyze the results in Fig. 1.31 for the bending mode. Solid curves *1* and *3* ($h_m \cdot h_r^{-1} = 1$ and 10) are curves of type *B* in Fig. 1.20; therefore, if $h_m \cdot h_r^{-1} = 1$ and 20, microbuckling in bending mode does not occur. Solid curves *4*, *5*, *6*, and *7* ($h_m \cdot h_r^{-1} = 20$, 30, 40, 50) are curves of type *A* in Fig. 1.20; therefore, if $h_m \cdot h_r^{-1} = 20$, 30, 40, 50, microbuckling occurs in bending mode. Thus, it was strictly proved that microbuckling in bending mode can or cannot occur depending on the structure of the composite laminate. As mentioned in Sec. 1.2.2.3 (qualitative contradiction 1), the approximate theories based of the first approach do not describe this phenomenon.

The following result is of interest too. It was strictly proved in [8, Vol. 1, Ch. 3] that the continuum theory of fracture (Sec. 1.2.3.2) follows as long-wave approximation (as the buckling wavelength tends to infinity) from the bending mode within the framework of the piecewise-homogeneous material model.

More details on the internal fracture of composite laminates can be found in [8, Vol. 1, Ch. 3].

1.2.3.3.2. Near-Surface Fracture. Let us briefly discuss results on the near-surface fracture of composite laminates obtained using the piecewise-homogeneous material model (see [8, Vol. 1, Ch. 5] for more details).

In studying surface instability, the composite laminate is assumed to occupy the lower half-space const $\geq x_2 > -\infty$ in the plane case (Fig. 1.25) and the lower half-space const $\geq x_3 > -\infty$ in the spatial case (Fig. 1.26). All the notation and reasoning stated in Sec. 1.2.3.3.1 before expression (1.12) also apply to near-surface fracture. Specific results were obtained for laminated composites with polymer or metal matrix (brittle or ductile fracture, respectively).

Two- and three-dimensional near-surface fracture problems are solved with (i) an exact method that reduces the problems to infinite systems of algebraic equations and (ii) an essentially approximate method that employs variational principles and the TLTSDB [6, 43].

In what follows, we will analyze results on near-surface instability in specific laminated composites with either polymer or metal matrix. We will restrict ourselves to the following qualitatively new phenomenon [8, Vol. 1, Ch. 5, p. 513]: surface instability does not occur at all concentrations of reinforcement and all relative stiffnesses. For example, as the external compressive load is continuously increased, internal instability may occur first or the critical loads for internal and surface instabilities may coincide.

This completes the brief discussion of results on near-surface fracture (near-surface instability) in laminated composite with polymer and metal matrices obtained within the framework of the piecewise-homogeneous material model. More details can be found in [8, Vol. 1, Ch. 5].

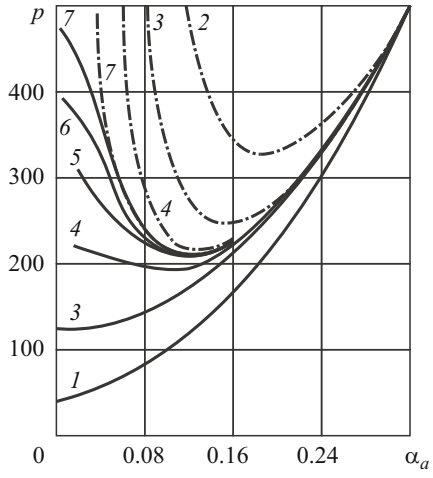

Fig. 1.31

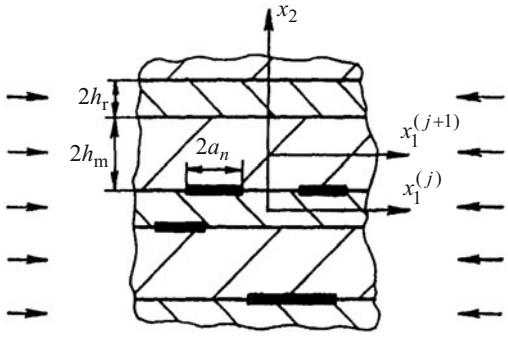

Fig. 1.32

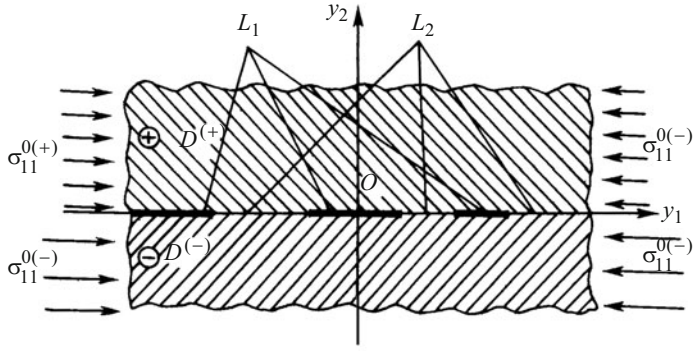

Fig. 1.33

1.2.3.3.3. Laminated Composites with Interfacial Defects. The TLTSDB [6, 43] and the piecewise-homogeneous material model were used to study the fracture of compressed laminated composites (microbuckling in composites) with interfacial defects of two types.

Defects of the first type are modeled by the absence of friction or imperfect bonding at the interface. In this case, the normal stresses and displacements are continuous at the interfaces, and it is also assumed that the shear stresses are zero at the interfaces. Such problems are solved using the general solutions of the static TLTSDB equations [6, 43], and the characteristic determinants are derived in explicit closed form. The roots of the characteristic equations are found numerically.

Defects of the second type are modeled by interface cracks. A design model for such problems is exemplified in Fig. 1.32 where the interaction of (micro)cracks located at different interfaces is generally taken into account.

Problems for composite laminates with interfacial defects of the second type (Fig. 1.32) can be solved only numerically (finite-difference method, finite-element method).

The exception is, apparently, microcracks located at the same interface. Note that microcracks do not interact with microcracks located at the neighboring parallel interfaces. The exact solution in closed form was obtained for microcracks located at the same interface, the corresponding design model being shown in Fig. 1.33 (see [8, Vol. 2, Ch. 8, pp. 168–199] for more details). The exact solution is found by using a general solution expressed in terms of functions of complex variables, introducing complex variables that include compressive stresses, and solving the problem of joining two holomorphic functions defined on the whole plane.

More details on the mechanics of fracture of compressed composite laminates modeled by a piecewise-homogeneous material can be found in [8, Vol. 1, Chs. 3 and 5; Vol. 2, Ch. 8, Sec. 2].

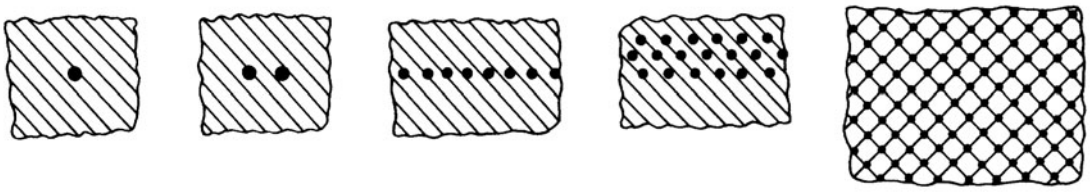

a *b* *c* *d* *e*

Fig. 1.34

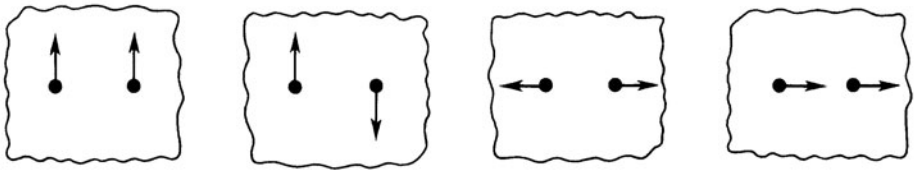

a *b* *c* *d*

Fig. 1.35

1.2.3.4. Unidirectional Fibrous Composites. Piecewise-Homogeneous Material. Here we will briefly discuss the mechanics of fracture of compressed unidirectional fibrous composites (Fig. 1.18) with polymer and metal matrices based on the piecewise-homogeneous material model. The TLTSDB [6, 43] is applied to each fiber and the matrix, and continuity conditions for stresses and displacements are prescribed at the interfaces. The basic results were obtained for brittle and ductile fracture. In the latter case, the generalized concept of increasing load outlined in, for example, the monographs [6, 43] was used. In line with the basic approach outlined in Sec. 1.2.3.1, it is necessary to analyze the static equations and boundary conditions of the TLTSDB [6, 43] for a piecewise-homogeneous material (eigenvalue problem). The basic results were obtained for microbuckling [8, Vol. 1, Ch. 4] and for near-surface buckling [8, Vol. 1, Ch. 6]. The list of references in [8] includes publications on stability of unidirectional fibrous composites analyzed using the second approach (as termed in Secs. 1.2.1 and 1.2.3.1 and in the monographs [7, 8]).

1.2.3.4.1. Internal Fracture. The internal instability of an unbounded unidirectional fibrous composite (Fig. 1.18) is analyzed using the general solutions of the static TLTSDB equations [6, 43] and the procedure outlined in Sec. 1.2.1, taking into account the approach corresponding to Fig. 1.20. It should be noted that here we discuss results for composites with no defects at the interfaces (continuity of stresses and displacements at the interfaces). Results for composites with interfacial defects are discussed in Sec. 1.2.3.4.3. As in (1.5), the indices "r" and "m" are used to refer to the reinforcement (filler, unidirectional fibers) and to the matrix (binder), respectively.

For unidirectional fibrous composites compressed along the fibers (Fig. 1.18), various problems arise depending on the structure of the composite in the cross-sectional plane and the design models used. Figure 1.34 (cross-sectional plane) shows the following design models.

1. One fiber (Fig. 1.34*a*); applied to fibrous composites with so low volume fraction of fibers that neighboring fibers do not interact.

2. Two fibers (Fig. 1.34*b*); applied to fibrous composites with so low volume fraction of fibers that two neighboring fibers can interact upon buckling due to the irregularity of the structure.

3. A periodic row of fibers (Fig. 1.34*c*); applied to fibrous composites of periodic structure such that upon buckling, fibers of the same row interact, whereas fibers in neighboring rows do not interact (rather short distances between fibers in the same row, rather long distances between neighboring rows).

4. Several periodic rows of fibers (Fig. 1.34*d*); applied to fibrous composites of periodic structure such that upon buckling, fibers in the same row interact, rows of fibers within a group of rows interact, and different groups of rows do not interact.

5. Doubly periodic array of fibers (Fig. 1.34*e*); applied to fibrous composites of doubly periodic structure with so short distances between neighboring fibers that upon buckling, the interaction of fibers should be described by the doubly periodic model.

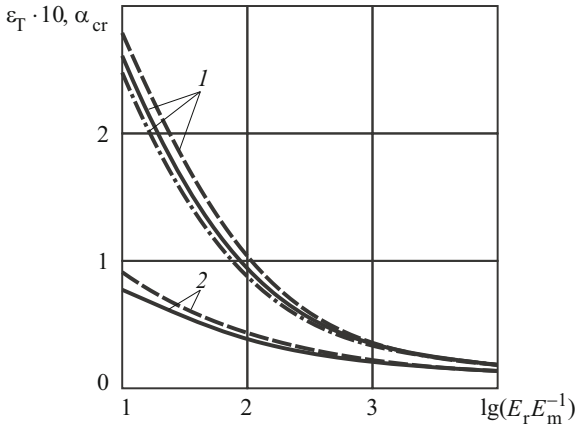

Fig. 1.36

The number of problems for unidirectional fibrous composites is determined by not only the number of design models (five models in Fig. 1.34), but also by the necessity of analyzing various buckling modes depending on cross-sectional symmetry. Certainly, after analyzing various buckling modes, it is necessary to minimize all the eigenvalues (usually the first eigenvalues for each buckling mode) to determine the critical shortening along the fibers.

Figure 1.35 shows (in the cross-sectional plane), as an example, various buckling modes for two fibers (Fig. 1.34*b*): in-phase out-of-plane buckling modes (Fig. 1.35*a*); antiphase out-of-plane buckling modes (Fig. 1.35*b*); antiphase in-plane buckling modes (Fig. 1.35*c*); in-phase in-plane buckling modes (Fig. 1.35*d*).

The general method for solving such problems, which was used to solve all problems of the internal fracture of unidirectional fibrous composites under uniaxial compression within the framework of the second approach, involves the following steps:

– application of the general solutions of the static TLTSDB equations [6, 43] in circular cylindrical coordinates to fibers and matrix;

– representation of the solution as the sum of solutions in local cylindrical coordinates in the form of Fourier series with undetermined coefficients, including special circular cylindrical functions;

– derivation of characteristic equations in the form of infinite characteristic determinants and explicit calculation of their elements;

– proving that these infinite characteristic determinants are normal for noninteracting fibers, which allows replacing infinite determinants with finite determinants to find the roots, i.e., to apply the method of truncation;

– proving the practical convergence of the method by comparing the roots obtained with increase in the order of truncated determinants.

This method helped to obtain numerous results on the internal fracture of compressed unidirectional fibrous composites with polymer and metal matrices (see [8, Vol. 1, Ch. 4] for a more detailed and consistent exposition of these results). Currently, these results appear the most accurate and rigorous. Moreover, the method allows refining results obtained for noninteracting fibers.

Let us now briefly discuss two examples from [8, Vol. 1, Ch. 4].

Example 1. Most results in [8, Vol. 1, Ch. 4] were obtained assuming homogeneous subcritical states under loading, as in Fig. 1.18. This assumption is valid when (i) the fibers and the matrix are incompressible and (ii) Poisson's ratios of the fibers and the matrix are equal ($\nu_r = \nu_m$). If Poisson's ratios of the fiber and matrix are different ($\nu_r \neq \nu_m$), the subcritical state will be inhomogeneous. This suggests that it is necessary to take into account (in buckling problems for unidirectional fibrous composites) the inhomogeneity of the subcritical state when $\nu_r \neq \nu_m$. This issue for one fiber (Fig. 1.34*a*) was examined in [8, Vol. 1, Ch. 4, Sec. 1, pp. 391–396]. Quite accurate results were obtained numerically for an inhomogeneous subcritical state. For example, Fig. 1.36 shows the dependence of $\varepsilon_T \cdot 10$ (ε_T is the theoretical ultimate strain) and $\alpha_{cr} = \pi R / l_{cr}$ (critical wave number $\alpha = \pi R / l$, R is the fiber cross-sectional radius, l is the buckling half-wavelength (along the fibers)) on $\lg(E_r \cdot E_m^{-1})$. Curves *1* correspond to α_{cr}, curves *2* to $\varepsilon_T \cdot 10$; the solid curves correspond to $\nu_r = 0.2$ and $\nu_m = 0.4$ (inhomogeneous subcritical

TABLE 1.1

Material	$(\Pi_3^-)_{ex}$, MPa			$(\Pi_3^-)_T$, MPa	
	2	min	Average	Continuum theory	Piecewise-homogeneous model
Annealed	965	501	665	736	958
Unannealed	1716	1049	1282	1467	1972

state), the dashed curves to $\nu_r = \nu_m = 0.2$ (homogeneous subcritical state), and the dash-and-dot curves to $\nu_r = \nu_m = 0.4$ (homogeneous subcritical state). Note that the solid and dash-and-dot lines for $\varepsilon_T \cdot 10$ practically coincide. The values $\nu_r = 0.2$ and $\nu_m = 0.4$ represent the case of the maximum difference between Poisson's ratios of typical reinforcements and matrices, according to [8, Vol. 1, Tables 0.1 and 0.2, p. 67 and p. 68].

Analyzing Fig. 1.36 and [8, Vol. 1, Table 4.1, p. 395], we conclude that when $E_r \cdot E_m^{-1} \geq 20$, tolerating an error 5% is sufficient to neglect the inhomogeneity of the subcritical state caused by the difference between Poisson's ratios of the reinforcement and the matrix and to assume that $\nu_r = \nu_m = 0.3$.

Example 2. Let us briefly discuss experimental and theoretical ultimate strengths for a VKA-1 metal-composite (unidirectional fibrous composite with aluminum matrix reinforced with 50% of boron fibers 140 μm in diameter; $S_r = S_m = 0.5$). Figure 1.24 shows specimens made of boron–aluminum composite. These results were reported in [52] and discussed in [8, Vol. 1, Ch. 4, pp. 486–488]. Note that ductile fracture was considered there and formulas (1.9) were used to describe the aluminum matrix. In fact, two metal-composites were considered: annealed and unannealed. In experiments, 32 annealed specimens and 14 unannealed specimens were destroyed to determine their experimental ultimate strengths. The theoretical ultimate strengths were determined using the continuum theory of fracture (Sec. 1.2.3.2), the piecewise-homogeneous material model for fibrous unidirectional composites (Sec. 1.2.3.4), and the doubly periodic design model (Fig. 1.34*e*). The results are summarized in Table 1.1 [8, Vol. 1, Ch. 4, Table 4.10, p. 487]. It can be seen that the continuum theory of fracture is in agreement with the average experimental results, while the of piecewise-homogeneous material model is in agreement with the maximum experimental results.

More details on the internal fracture of unidirectional fibrous composites can be found in [8, Vol. 1, Ch. 4].

1.2.3.4.2. Near-Surface Fracture. Let us briefly discuss results on the near-surface fracture of unidirectional fibrous composites obtained using the piecewise-homogeneous material model (see [8, Vol. 1, Ch. 6] for more details).

To study surface instability, a fibrous unidirectional composite occupying a half-space with the boundary surface parallel to the fibers is considered (Fig. 1.18). In this connection, the cross-section of the composite is a half-plane (Fig. 1.37) whose structure depends on which of the typical design models is usec. Figure 1.37 shows five typical design models that can be described in a similar way as in Sec. 1.2.3.4.1. Note that the full circles in Fig. 1.37, as well as in Figs. 1.34 and 1.35, represent fiber cross-sections. The surface instability of unidirectional fibrous composites is studied by analyzing buckling modes that decay with distance from the boundary of the lower half-space (Fig. 1.37), which is determined by an additional condition. The solution is formed by adding a term in the form of a Fourier transform to the solution in 1.2.3.4.1 to satisfy the boundary conditions on the boundary of the lower half-space. With such a candidate solution, the method described before Example 1 in Sec. 1.2.3.4.1 was used.

Specific results on near-surface fracture were obtained for unidirectional fibrous composites with polymer and metal matrices. More details can be found in [8, Vol. 1, Ch. 6].

1.2.3.4.3. Unidirectional Fibrous Composites with Interfacial Defects. Let us briefly discuss results on the internal and near-surface fracture of unidirectional fibrous composites with interfacial defects of the first and second types (defined in Sec. 1.2.3.3.3) under compression.

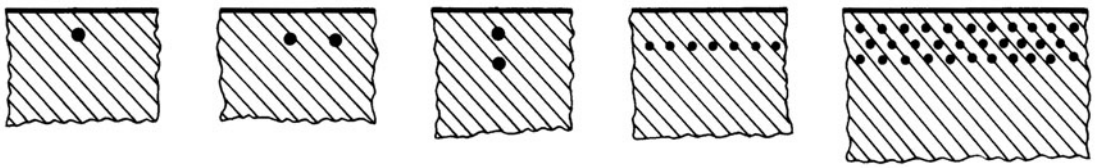

a *b* *c* *d* *e*

Fig. 1.37

For defects of the first type, results are obtained for one fiber and can be found in [8, Vol. 1]. For internal fracture, results were obtained using the design model shown in Fig. 1.34*a* and are presented in [8, Vol. 1, pp. 415–417]. For near-surface fracture, results were obtained using the design model shown in Fig. 1.37*a* and are presented in [8, Vol. 1, pp. 561–563].

For defects of the second type (at cylindrical interfaces in unidirectional fibrous composites), no results have been published yet.

More details on the mechanics of fracture of compressed unidirectional fibrous composites modeled by a piecewise-homogeneous material can be found in [8, Vol. 1, Chs. 4 and 6].

1.2.3.5. More General Buckling Modes. Piecewise-Homogeneous Material. Here we will discuss general and specific results on more general buckling modes (in the internal structure of laminated and fibrous composites) in comparison with the buckling modes analyzed in Secs. 1.2.3.3 and 1.2.3.4.

1.2.3.5.1. Generalities. In studying stability of laminated (Sec. 1.2.3.3) and unidirectional fibrous (Sec. 1.2.3.4) composites modeled by a piecewise-homogeneous material based on the TLTSDB [6, 43], the factor $\sin \pi l^{-1} x_3$ is separated out in all buckling modes, where the coordinate x_3 is measured along the fibers or plies and l is the buckling half-wavelength along fibers or plies. Thus, the infinite-fiber model was used assuming that each fiber or ply buckles in the same periodic mode along fibers or plies. That such buckling modes occur was confirmed by experiments on composites with polymer (epoxy resin) matrix reinforced with glass fibers (Fig. 1.2) or with carbon fibers (Fig. 1.3).

The planes of equal phase in such buckling modes (along the x_3-axis; along fibers or plies) are perpendicular to the Ox_3-axis (perpendicular to fibers or plies). In this connection, it may be considered that fracture propagates along these planes. In a sense, the validation of the above procedure regarding buckling modes is the rigorous proof (Sec. 1.2.3.2.1), based on the continuum theory of fracture (Sec. 1.2.3.2), of the fact that brittle fracture propagates along planes perpendicular to the line of action of compressive loads. Note that the continuum theory of fracture (Sec. 1.2.3.2) assumes compression in the direction of preferred reinforcement (along fibers or plies). Nevertheless, the use of the continuum theory to prove an element of the piecewise-homogeneous material model is insufficiently logical and consistent because the continuum theory of fracture is approximate and less accurate than the piecewise-homogeneous material model.

In this connection, it appears reasonable to develop a method that would allow analyzing more general buckling modes in laminated and unidirectional fibrous composites than the buckling modes addressed in Secs. 1.2.3.3 and 1.2.3.4. Certainly, along with development of this method, it is necessary to analyze specific classes of problems to formulate general conclusions.

A method for studying more general buckling modes was proposed in [42] for unidirectional fibrous composites (Fig. 1.18) with the most complex doubly periodic structure (Fig. 1.34*e*) and in [46] for laminated composites (Fig. 1.19). This method [42, 46] assumes that fibers or plies are infinitely long along the Ox_3-axis, compression is along the Ox_3-axis, and the buckling modes are periodic along the Ox_3-axis. In Secs. 1.2.3.3 and 1.2.3.4, it was additionally assumed that all reinforcement elements (plies or fibers) buckle in phase or that neighboring reinforcement elements buckle in antiphase. The method from [42, 46] does not use such an assumption, which is why the buckling modes addressed in [42, 46] can be considered more general.

For more accurate characterization of the buckling modes considered in [42, 46] and being periodic along the Ox_3-axis, use is made of the concept of plane Π that consists of points of the buckled composite that are in phase along the Ox_3-axis. The first octant of the plane Π in Fig. 1.38 is hatched and is defined by a unit vector n with the following components:

$$n_1,\ n_2,\ n_3, \quad n_1^2 + n_2^2 + n_3^2 = 1. \tag{1.13}$$

In [42, 46], solutions of the system of the static TLTSDB equations [6, 43] were found in explicit form for an arbitrary position of the plane Π (Fig. 1.38) defined by the unit vector n. These solutions were constructed for unidirectional fibrous

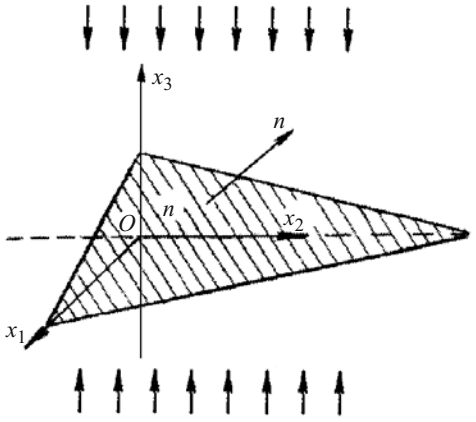

Fig. 1.38

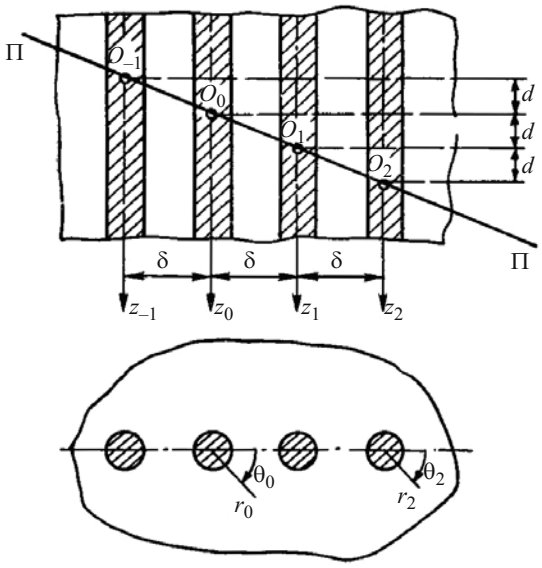

Fig. 1.39

composites of the most complex doubly periodic structure (Fig. 1.34*e*), which, certainly, can be reduced to simpler structures (Fig. 1.34*a–d*), and for laminated composites (Figs. 1.19, 1.25, and 1.26). In [42], it was pointed out that for an arbitrary position of the plane Π in unidirectional fibrous composites, the characteristic equation has the form of an infinite determinant. It was also proved that the infinite determinant is normal for noninteracting fibers, which means that it is possible to truncate the determinant to find the roots numerically. Practical convergence can be achieved by increasing the order of the truncated determinant and comparing the results obtained. In [46], it was pointed out that the characteristic determinant for laminated composites is of finite order and its elements are represented in closed form.

Note that the methods of Secs. 1.2.3.3 and 1.2.3.4 follow from the methods of [42, 46] if

$$n_1 = 0,\ n_2 = 0,\ n_3 = 1 \tag{1.14}$$

in (1.13). In this case, the plane Π is perpendicular to the Ox_3-axis (perpendicular to the line of action of the compressive load).

After finding the roots of the characteristic determinants [42, 46], it is necessary to minimize them (to find the critical values) with respect to the following parameters: l is the buckling half-wavelength along the Ox_3-axis; n_1, n_2, and n_3 are the parameters defining the position of the plane Π. For this purpose, it is possible first to determine l_{cr} at values (1.14) and then to analyze the variation in parameters of interest $((\Pi_3^-)_T, \varepsilon_T)$ at $l = l_{cr}$ and different values of n_1, n_2, and n_3 (1.13).

1.2.3.5.2. Results for Unidirectional Fibrous Composite. Results for a unidirectional fibrous composite modeled as in Fig. 2.34*c* (one infinite periodic row of fibers) are published in [55, 56, 58]. The design model for the case of an arbitrary position of the plane Π is shown in Fig. 1.39.

The cross-section of a composite with one periodic row of fibers is shown in the lower part of Fig. 1.39. The upper part of Fig. 1.39 corresponds to the plane that passes through the axes of the fibers in the infinite periodic row. The following notation is used in Fig. 1.39: R is the fiber radius; δ is the distance between two neighboring fibers; d is the phase shift along fibers within a buckling mode; l is the buckling half-wavelength along the fibers. Note that if $d = 0$ in Fig. 1.39, then we have the case (1.14) where the plane Π is perpendicular to the fibers, which was assumed in Sec. 1.2.3.4.

In [58], fibers and matrices were modeled by linear elastic bodies with $\nu_r = \nu_m$ and the following parameter values were used:

$$\begin{aligned} &E_r \cdot E_m^{-1} = 50,\ 100,\ 200,\ 500,\ 1000, \\ &\delta \cdot R^{-1} = 2.5,\ 3,\ 4,\ 5,\ 7,\ 15, \\ &d \cdot l^{-1} = 0,\ 0.25,\ 0.5,\ 0.75,\ 1. \end{aligned} \tag{1.15}$$

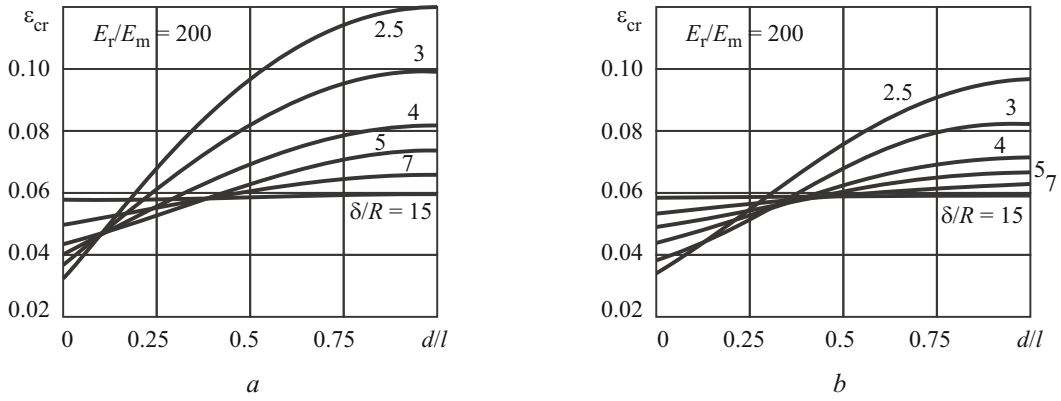

Fig. 1.40

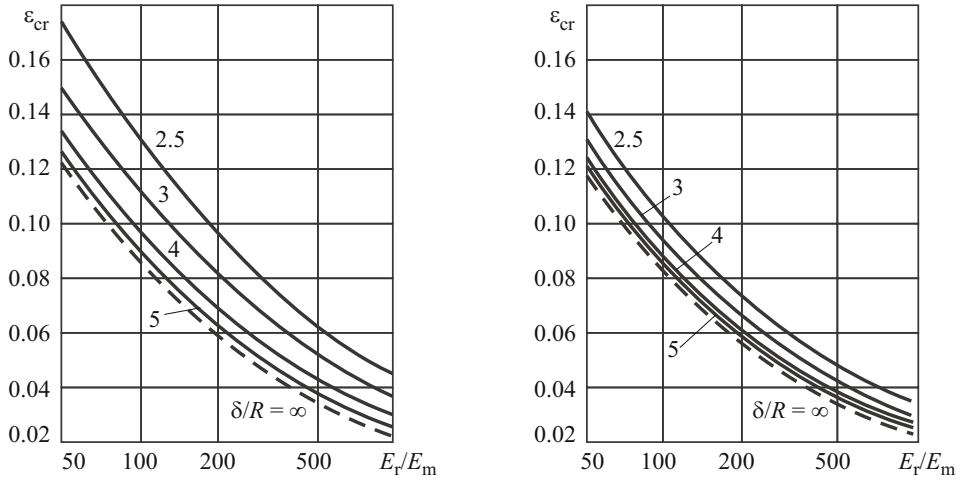

Fig. 1.41

Figure 1.40 shows the dependence of ε_{cr} (critical shortening along fibers) on $d \cdot l^{-1}$ (deviation of the plane Π from the plane perpendicular to the fibers) for different distances $\delta \cdot R^{-1}$ between neighboring fibers for $E_r \cdot E_m^{-1} = 200$. Figure 1.40*a* represents in-plane buckling as in Fig. 1.35*c* and *d*, and Fig. 1.40*b* represents out-of-plane buckling as in Fig. 1.35*a* and *b*.

In minimizing ε_{cr} (Fig. 1.40) with respect to $d \cdot l^{-1}$ for in-plane buckling (Fig. 1.40*a*) and out-of-plane buckling (Fig. 1.40*b*), we obtain

$$\varepsilon_T = \varepsilon_{cr} \quad \text{at} \quad d \cdot l^{-1} = 0. \tag{1.16}$$

Thus, the plane Π (Fig. 1.38) is perpendicular to the fibers, as in Sec. 1.2.3.4, i.e., which confirms the generality of the method described in Secs. 1.2.3.3 and 1.2.3.4. The above conclusion was drawn after analysis of only one example. In this connection, this conclusion should be validated against other internal and near-surface fracture problems for laminated and unidirectional fibrous composites.

To illustrate the effect of change in the relative stiffness of fibers and matrix ($\nu_r = \nu_m$) on ε_{cr}, Fig. 1.41 shows the plot of $\varepsilon_{cr} = \varepsilon_{cr}(E_r \cdot E_m^{-1})$ obtained in [58] for $d \cdot l^{-1} = 0.5$ and different values of $\delta \cdot R^{-1}$ (the notation being the same as in Fig. 1.39).

Figure 1.41*a* represents in-plane buckling as in Fig. 1.35*c* and *d*, and Fig. 1.41*b* represents out-of-plane buckling as in Fig. 1.35*a* and *b*. The solid curves in Fig. 1.41 correspond to $\delta \cdot R^{-1} = 2.5, 3, 4, 5$, the dashed curve represents the case $\delta \cdot R^{-1} = \infty$ (one fiber; design model shown in Fig. 1.34*a*), and a log scale is used for the axis $E_r \cdot E_m^{-1}$. It follows from Fig. 1.41*a*, *b* that the parameter $E_r \cdot E_m^{-1}$ has a strong effect on ε_{cr}.

TABLE 1.2

E_r / E_m	In-plane			Out-of-plane		
	Number of equations	$\delta / R = 2.5$	$\delta / R = 4$	Number of equations	$\delta / R = 2.5$	$\delta / R = 4$
50	22	1740	1346	20	1450	1275
	34	1750	1346	32	1452	1275
200	10	820	671	8	718	624
	22	972	693	20	756	628
	34	981	694	32	757	627
1000	10	377	300	8	328	273
	22	465	315	20	347	274
	34	469	315	32	348	274

It should be noted that the method proposed in [42] and intended to study the internal instability of unidirectional fibrous composites allows finding the roots of infinite determinants. In [42], it is pointed out that these infinite determinants are normal (for noninteracting fibers). Thus, infinite determinants can be truncated to find their roots numerically. In this connection, the practical convergence of the method is usually proved by analyzing the change in the roots with increasing order of characteristic determinants obtained by truncating infinite characteristic determinants.

In [58], the case of one infinite periodic row of fibers (Fig. 1.39) was considered, and numerical results were obtained by modeling the matrix and fibers with $\nu_r = \nu_m$ as in Sec. 1.2.3.5.2. Table 1.2 summarizes, following [58], values of $\varepsilon_{cr} \cdot 10^4$ (ε_{cr} is the critical shortening along the fibers) for $d \cdot l^{-1} = 0.5$ (d is specified in Fig. 1.39, l is the buckling half-wavelength along the fibers) for different values of $\delta \cdot R^{-1}$ and $E_r \cdot E_m^{-1}$. The values of $\varepsilon_{cr} \cdot 10^4$ were calculated using different number of equations (also indicated in Table 1.2), which represents the order of the truncated characteristic determinant.

It follows from Table 1.2 that for the stiffness and geometry used, sufficient accuracy can be achieved with a determinant of the 22nd order for in-plane buckling and a determinant of the 20th order for out-of-plane buckling, because using determinants of the 34th and 32nd orders, respectively, affects only the third decimal place. The case $\delta \cdot R^{-1} = 2.5$ represents closely spaced fibers (the distance (matrix) between fibers is fiber half-radius).

In summary, it makes sense to point out that the analysis made in this section is more detailed than in Secs. 1.2.3.3 and 1.2.3.4 because the results discussed in this section were not included in the monograph [8].

1.2.4. Analysis of Theoretical Results. On Study of the Kinking Phenomenon. We will briefly discuss, following [8, Vol. 1, pp. 72–74], studies of the kinking phenomenon, a concept especially popular among English-speaking researchers.

The kinking phenomenon was for the first time addressed in the paper [31] published in 1983 and in some other publications. Studies on kinking were reviewed in [32, 33, 40] of which [40] was published in *Advances in Applied Mechanics* (Vol. 33, pp. 43–119) in 1997 and [33] was published in *Applied Mechanics Reviews* in 1994. The results partially addressed in Secs. 1.2.3.3 and 1.2.3.4 were also reviewed *Applied Mechanics Reviews* [65] in 1992.

Kinking is manifested as narrow kink bands of destroyed material occurring in a composite compressed along the reinforcement. The kinking phenomenon is schematized in Fig. 1.42 [33, Fig. 2, p. S247], where W is the width of the kink band. Kink bands are usually analyzed using quite approximate formulas.

Figure 1.42 represents an already destroyed specimen; The beginning (start) of fracture is unclear; therefore, it may be expected that fracture begins with microbuckling. It should also be noted that kinking caused by compression along the

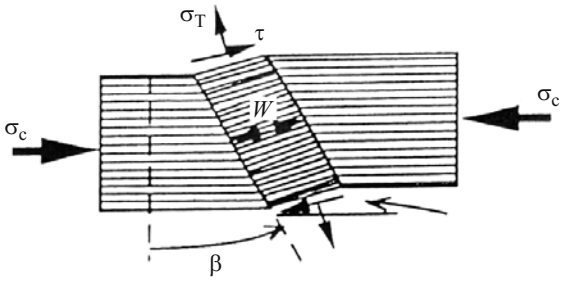

Fig. 1.42

horizontal axis (Fig. 1.42) is accompanied by displacement of the material on both sides of the kink band along the vertical axis (Fig. 1.42), which is a typical feature of the kinking phenomenon.

Some considerations on the occurrence of kinking were given in [47] and in [8, Vol. 1, pp. 73–74]. Some considerations from [8] are given below.

1. Kinking (Fig. 1.42) can occur if the boundary conditions for a specimen compressed along the horizontal axis allow displacements along the vertical axis.

2. An isolated kink band cannot occur during internal fracture in an unbounded material compressed along the axes of material symmetry (in continuum approximation). Inside a composite compressed along the axes of material symmetry, only alternating kink bands can exist to balance the disturbed stress–strain state.

3. By analyzing the kinking phenomenon, it is, apparently, impossible to uniquely identify the mechanisms responsible for the beginning (start) of fracture. One of such mechanisms may be microbuckling. It can be studied using the TLTSDB [6, 43].

As already mentioned in [8, Vol. 1, p. 73], the above considerations are just the point of view of [8, 47]. In this connection, there may be other considerations.

The second consideration is in a sense validated by the experimental results reported in [74] and presented in Fig. 1.14. These experimental results were discussed in Sec. 1.1.2 near Fig. 1.14.

This completes the brief discussion of the kinking phenomenon.

1.3. Conclusions to Sec. 1. Section 1 has provided a brief historical sketch of experimental and theoretical studies on microbuckling in and subsequent fracture of composites under compression. The theoretical studies were based on the infinite-fiber model. The following conclusions can now be made.

1. The experimental results discussed prove that microbuckling may occur in composites with quite long reinforcement elements, which are studied using the infinite-fiber model, and in composites with relatively short reinforcement elements, which are studied using the finite-fiber model.

2. Only theoretical results obtained with the infinite-fiber model have been analyzed. These results were obtained using either various approximate assumptions or the three-dimensional linearized theory of stability of deformable bodies (TLTSDB) [6, 43].

3. This brief historical sketch has not involved the mathematics used to solve specific classes of problems. This kind of exposition allows a wide range of researchers to gain insight into various aspects of the issue.

2. Finite-Fiber Model in the Three-Dimensional Theory of Stability of Composites. Analysis of Approaches and Results. We will discuss results on internal instability and near-surface instability of composites compressed along the reinforcement obtained using the finite-fiber model and the TLTSDB [6, 43]. The studies were conducted assuming plane strain. In this connection, the results to be discussed may be considered to represent infinitely long bands (infinite in the direction perpendicular to the plane of interest) of finite width, i.e., ribbon-reinforced composite laminates. Since the finite-fiber model is used in this section (unlike Sec. 1.2), the subcritical state is inhomogeneous and it is necessary to use numerical methods.

According to the basic assumption of the approximate approach [26, 67] formulated in Sec. 1.2.2.2, a unidirectional fibrous composite is modeled by a composite laminate under plane strain conditions. In this connection, we will use terminology typical for the theory of stability of unidirectional fibrous composites. Such results are included in well-known fundamental multivolume monographs on fracture [25] and on composites [19] and cited in later publications without any comments (see Sec. 1.2.2.2 for more details).

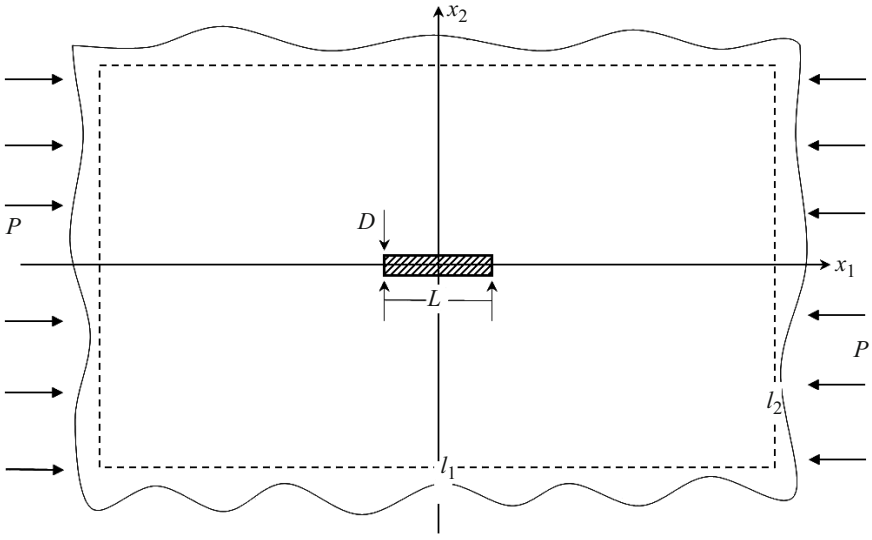

Fig. 2.1

It should be noted that the above-mentioned modeling and terminology will be used only to interpret the results, which were obtained using the piecewise-homogeneous material model and the TLTSDB [6, 43] for composites reinforced with relatively short fibers (finite-fiber model).

2.1. Principles of the Finite-Fiber Model. We will briefly outline the principles of the theory of stability that allows adequate description of the buckling of composites reinforced with fibers of finite length under compression along the reinforcement. We will discuss the basic equations and relations of the three-dimensional linearized theory of stability of deformable bodies at small initial strains, approaches to the selection of models for the description of the mechanical properties of composites, to mathematical formulation of differential problems, and microbuckling criteria.

The principles of the theory of stability of finite fibers in a matrix used to formulate problems and its applicability limits can be formulated as follows.

1. The matrix and fibers are modeled by linear elastic isotropic bodies, which is justified for relatively short-term external loads and moderate temperatures.

2. Use is made of the second theory of small subcritical deformations of the three-dimensional linearized theory of stability when the initial state is determined by a geometrically linear theory. This approach is considered valid for relatively stiff fibrous composites that undergo fracture at relatively small strains.

3. The external loads are considered to be "dead," which means that the sufficient applicability conditions for the static TLTSDB method are satisfied and this method can be used in all studies.

4. The reinforcement and the matrix are assumed perfectly bonded (the stress and displacement vectors are continuous at the interfaces) in either determining the subcritical state or solving buckling problems.

5. When the number of fibers is finite, decay at infinity is assumed. For a periodic system of fibers, periodicity conditions are additionally prescribed.

6. All studies are carried out assuming plane strain: a longitudinal section of fibrous materials passing through the axis of fibers in one plane is considered.

2.1.1. Problem Statement. Thus, plane strain in the plane x_1Ox_2 is assumed, the TLTSDB for small subcritical strains is used, and the reinforcement and matrix are modeled by elastic isotropic bodies. Use is made of Lagrangian coordinates that coincide with Cartesian coordinates before deformation. Figure 2.1 shows a design model for the elementary case of fibers that do not interact with each other through the matrix before and during buckling. Such a situation occurs when the volume fraction of the reinforcement is relatively small.

Since we are considering a longitudinal section of fibrous materials that runs through the axis of fibers lying in one plane, the three-dimensional problem (for cylindrical fibers of finite length) is, in fact, reduced to a plane problem (for plies of finite sizes). This procedure, as already mentioned above, is consistent with the basic assumption of the approximate approach [26, 67] formulated in Sec. 1.2.2.2. This procedure may be considered an approximate approach to the interpretation of results

because no modeling or similarity criteria have not applied and analyzed for half a century now (the paper [67] was published in English in 1965). The results from [26, 67] were included in well-known encyclopedic monographs on composites and fracture.

The subcritical state is analyzed using the classical linear theory of isotropic elasticity; the corresponding equilibrium equations and constitutive equations have the following form (the index "0" is used to refer to the initial (subcritical) state; the indices "r" and "m" refer to the fibers and matrix, respectively):

$$\frac{\partial}{\partial x_i}\sigma_{ij}^0 = 0,$$

$$\sigma_{ij}^0 = \delta_{ij}\lambda\varepsilon_{nn}^0 + 2\mu\varepsilon_{ij}^0,$$

$$2\varepsilon_{ij}^0 = \frac{\partial u_i^0}{\partial x_j} + \frac{\partial u_j^0}{\partial x_i}. \tag{2.1}$$

Since the matrix is considered unbounded, it is convenient to represent the stresses and displacements as the sums of the stresses and displacements induced by the external load applied to the matrix at infinity and the to perturbations of the stress–strain state caused by the presence of a fiber of finite length:

$$\sigma_{ij}^{0\mathrm{m}} = \sigma_{ij}^{\infty} + \sigma_{ij}^{10\mathrm{m}},$$

$$u_j^{0\mathrm{m}} = u_j^{\infty} + u_j^{10\mathrm{m}}, \tag{2.2}$$

where

$$\sigma_{11}^{\infty} = -P, \quad \sigma_{22}^{\infty} = 0, \quad \sigma_{12}^{\infty} = 0,$$

$$u_1^{\infty} = A_1 x_1, \quad u_2^{\infty} = A_2 x_2. \tag{2.3}$$

The subcritical state is determined using the basic relations that include the following continuity conditions for the stress and displacement vectors at the interfaces between the composite components:

$$\sigma_{11}^{\infty} + \sigma_{11}^{10\mathrm{m}} = \sigma_{11}^{0\mathrm{r}}, \quad \sigma_{12}^{10\mathrm{m}} = \sigma_{12}^{0\mathrm{r}}, \quad u_j^{\infty} + u_j^{10\mathrm{m}} = u_j^{0\mathrm{r}}, \quad x_1 = \pm L/2, \quad |x_2| \le \pm D/2, \tag{2.4}$$

$$\sigma_{22}^{10\mathrm{m}} = \sigma_{22}^{0\mathrm{r}}, \quad \sigma_{12}^{10\mathrm{m}} = \sigma_{12}^{0\mathrm{r}}, \quad u_j^{\infty} + u_j^{10\mathrm{m}} = u_j^{0\mathrm{r}}, \quad |x_1| \le \pm L/2, \quad x_2 = \pm D/2, \tag{2.5}$$

and the conditions of decay at infinity

$$\sigma_{ij}^{10\mathrm{m}} \to 0, \quad u_j^{10\mathrm{m}} \to 0 \quad \text{as} \quad \sqrt{x_1^2 + x_2^2} \to \infty. \tag{2.6}$$

The buckling problem is solved using the static TLTSDB method and the second theory of small subcritical deformations; the reinforcement and the matrix are modeled by linear elastic isotropic bodies, which is consistent with the problem of determining the subcritical stress–strain state. Thus, the equilibrium equations and the components of the asymmetrical stress tensor can be represented as

$$\frac{\partial}{\partial x_i}\left(\omega_{ij\alpha\beta}\frac{\partial}{\partial x_\beta}u_\alpha\right) = 0, \quad t_{ij} = \omega_{ij\alpha\beta}\frac{\partial}{\partial x_\beta}u_\alpha, \quad i, j, \alpha, \beta = 1, 2, \tag{2.7}$$

the components of the tensor ω are expressed as

$$\omega_{ij\alpha\beta} = \delta_{ij}\delta_{\alpha\beta}\lambda + (\delta_{i\beta}\delta_{\alpha j} + \delta_{i\alpha}\delta_{\beta j})\mu + \delta_{\alpha j}\sigma_{i\beta}^0, \quad \sigma_{i\beta}^0 = \delta_{i\beta}\sigma_{\beta\beta}^0, \tag{2.8}$$

where λ and μ are the Lame constants.

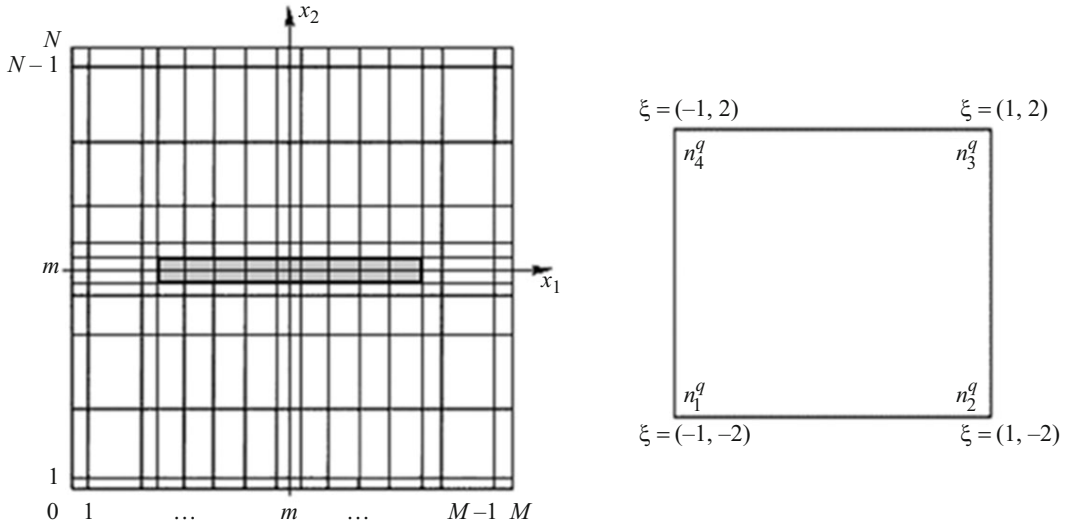

Fig. 2.2

In solving buckling problems, the basic relations (2.7) should be applied separately to the matrix, writing them for σ_{ij}^{1m}, ε_{ij}^{1m}, and u_j^{1m}, and for $\omega_{ij\alpha\beta}^{1m}$, λ_m, and μ_m and separately to the fiber, writing them for σ_{ij}^{r}, ε_{ij}^{r}, and u_j^{r} and for $\omega_{ij\alpha\beta}^{r}$, λ_r, and μ_r. Thus, according to (2.2), (2.3), (2.8), we have the following expressions for the matrix and fiber, respectively:

$$\omega_{ij\alpha\beta}^{1m} = \delta_{ij}\delta_{\alpha\beta}\lambda_m + (\delta_{i\beta}\delta_{\alpha j} + \delta_{i\alpha}\delta_{\beta j})\mu_m + \delta_{\alpha j}\sigma_{i\beta}^{0m},$$

$$\sigma_{i\beta}^{0m} = -\delta_{i\beta}\delta_{\beta 1}P + \sigma_{i\beta}^{10m}, \tag{2.9}$$

$$\omega_{ij\alpha\beta}^{r} = \delta_{ij}\delta_{\alpha\beta}\lambda_r + (\delta_{i\beta}\delta_{\alpha j} + \delta_{i\alpha}\delta_{\beta j})\mu_r + \delta_{\alpha j}\sigma_{i\beta}^{0r}. \tag{2.10}$$

The complete statement of the buckling problem also includes the following continuity conditions for the stress and displacement vectors at the interfaces:

$$t_{11}^{1m} = t_{11}^{r}, \quad t_{12}^{1m} = t_{12}^{r}, \quad u_1^{1m} = u_1^{r}, \quad u_2^{1m} = u_2^{r}, \quad x_1 = \pm L/2, \quad |x_2| \le \pm D/2, \tag{2.11}$$

$$t_{22}^{1m} = t_{22}^{r}, \quad t_{21}^{1m} = t_{21}^{r}, \quad u_1^{1m} = u_1^{r}, \quad u_2^{1m} = u_2^{r}, \quad |x_1| \le \pm L/2, \quad x_1 = \pm D/2, \tag{2.12}$$

and the following conditions of decay at infinity:

$$u_j^{1m} \to 0 \quad \text{as} \quad \sqrt{x_1^2 + x_2^2} \to \infty. \tag{2.13}$$

It should be noted that the subcritical state in the situation shown in Fig. 2.1 is similar to the problem of the stress concentration (under axial loading) near a rectangular inclusion filled with a dissimilar material. In this case, the subcritical state is essentially inhomogeneous, depending on the two variables x_1 and x_2.

Thus, in solving buckling problems using the TLTSDB (second theory of small subcritical deformations) and assuming plane strain, we arrive at an eigenvalue problem for a system of partial differential equations with variable coefficients dependent on x_1 and x_2. This eigenvalue problem cannot be solved analytically, and numerical methods should be used.

2.1.2. Numerical Method. The problems formulated are solved using the finite-difference method, the variational difference method, and the concept of reference schemes. This approach was detailed in the review [63] with reference to wide classes of problems of composite mechanics.

Using the notation introduced in Fig. 2.1, we will discuss the main steps of the numerical method. The infinite domain is replaced by a finite rectangular domain with side lengths $l_1 \times l_2$. To determine the subcritical state and to solve the buckling problem, the condition of decay at infinity is replaced by similar conditions of decay on the boundary of the rectangle. The dimensions of the external rectangle $l_1 \times l_2$ are chosen by way of computational experiments so that their further increase does not effect the results.

The rectangle $l_1 \times l_2$ is covered by straight lines parallel to the coordinate axes $x_1 = \text{const}$ and $x_2 = \text{const}$ to form a doubly nonuniform difference mesh $\overline{\omega} = \omega \cup \gamma$, where ω is the set of internal nodes and γ is the set of boundary nodes (Fig. 2.2). The mesh is such that the material can be considered homogeneous within each cell. The mesh can be refined where the material properties change sharply, as along the interfaces between the composite components. Thus, the mesh consisting of internal and boundary nodes is a set of rectangular cells that have mechanical and geometric characteristics of the composite component contained in them.

Discrete problems over the mesh $\overline{\omega}$ are formulated using the variational difference method and the concept of reference schemes. The components of reference schemes are determined by approximating and minimizing the appropriated functional on a cell template. When applying this procedure to buckling problems, the variational principles of the TLTSDB are used. Summing the values of reference schemes at each node of the mesh, we arrive at difference problems that are discrete analogs of the corresponding continuous problems.

Thus, the difference problem in operator form that should be solved to determine the subcritical stress–strain state and corresponds to the problem of linear elasticity (2.1)–(2.6) can be formulated as follows:

$$\mathbf{Au} = \mathbf{\Phi}, \quad \mathbf{x} \in \overline{\omega} \quad \text{or} \quad A_i \mathbf{u} = \Phi_i, \quad \mathbf{x} \in \overline{\omega}. \tag{2.14}$$

The expressions of difference operators are obtained by summing the values of reference schemes at each node of the mesh:

$$A_i \mathbf{u} = \sum_{\xi \in \mathbf{X}} a_i(\xi)\mathbf{u}, \qquad \Phi_i = \sum_{\xi \in \mathbf{X}} \varphi_i(\xi), \qquad \mathbf{x} \in \overline{\omega}. \tag{2.15}$$

The reference operators obtained on a cell template are expressed as

$$a_i(\xi)\mathbf{u} = -H \frac{\sigma_{ji} + \sigma_{ji}^{\xi_j}}{\eta_{\xi_j}}, \quad \mathbf{x} \in \overline{\omega},$$

$$\varphi_i(\xi) = -\frac{2H}{\eta_{\xi_j}} P_1, \quad \mathbf{x} \in \gamma, \tag{2.16}$$

where $H = h_1 h_2$ is the cell area, $h_i = \eta_{\xi_i}$ sign $\xi_i > 0$.

Hereafter, the sum sign means that the values of the reference operator at the node $\mathbf{x} \in \overline{\omega}$ are summed for those parameters ξ that correspond to the node $\mathbf{x}$ in all adjacent cells.

Note that the difference operator of problem (2.14) preserves the properties of self-adjointness and positive definiteness of the differential operator. Thus, the subcritical stress–strain state is determined by solving Eqs. (2.14), which can be represented as a system of linear equations with symmetric matrix.

The difference problem corresponding to the differential problem (2.7)–(2.13) can be represented in operator form as

$$\mathbf{Au} = p\mathbf{Bu}, \quad \mathbf{x} \in \overline{\omega} \quad \text{or} \quad A_i \mathbf{u} = pB_i \mathbf{u}, \quad \mathbf{x} \in \overline{\omega}. \tag{2.17}$$

The expressions of difference operators are obtained by summing the values of reference schemes at each node of the mesh:

$$A_i \mathbf{u} = \sum_{\xi \in \mathbf{X}} a_i(\xi)\mathbf{u}, \quad B_i \mathbf{u} = \sum_{\xi \in \mathbf{X}} b_i(\xi)\mathbf{u}, \quad \mathbf{x} \in \overline{\omega}. \tag{2.18}$$

The reference operators obtained on a cell template are expressed as

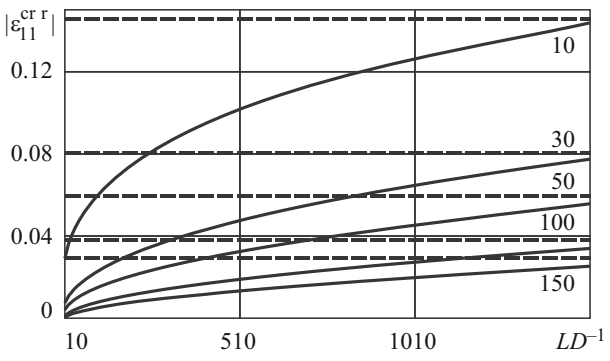

Fig. 2.3

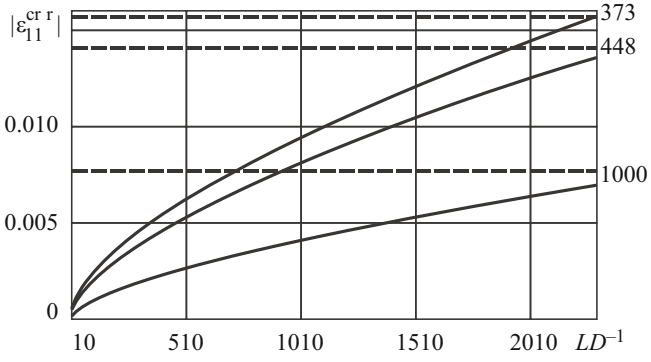

Fig. 2.4

$$a_i(\xi)\mathbf{u} = -H\frac{\sigma_{ji} + \sigma_{ji}^{\xi_j}}{\eta_{\xi_j}}, \quad b_i(\xi)\mathbf{u} = -H\frac{\sigma_{jk}^0 u_{i,\xi_k} + (\sigma_{jk}^0 u_{i,\xi_k})^{\xi_j}}{\eta_{\xi_j}}, \quad \mathbf{x} \in \overline{\omega}, \tag{2.19}$$

where $H = h_1 h_2$ is the cell area, $h_i = \eta_{\xi_i}$ sign $\xi_i > 0$.

The difference operators of problem (2.17) preserve the properties of self-adjointness and positive definiteness of the corresponding differential operators. Thus, the buckling problem is solved by solving Eqs. (2.17), which can also be represented as a generalized algebraic eigenvalue problem.

This approach to difference problems considerably simplifies the numerical procedure because general expressions of reference operators can be applied to all problems of the class in question. Moreover, the above method of summing the values of reference operators obtained on a cell template applies to all classes of problems and allows automating the process of constructing algebraic problems. To solve algebraic problems, direct and iterative methods well known in the theory of difference schemes are used, such as the Cholesky method, the conjugate-gradient method, the subspace-iteration method, the gradient-descent method.

2.1.3. Asymptotic Passage to the Infinite-Fiber Model. Let us compare results on buckling of polymer-matrix composites obtained using the finite-fiber (Fig. 2.1) and infinite-fiber (Fig. 1.19) models. The assumption of plane strain in the plane x_1Ox_2 (Figs. 2.1 and 1.19) is made. We will discuss the numerical results from [9, 52] with reference to the finite-fiber model and the results from [8] with reference to the infinite-fiber model. All the results were obtained using the second three-dimensional linearized theory of stability of deformable bodies [6, 43] and the assumption of small subcritical strains, determining the initial state from the geometrically linear theory, and modeling the reinforcement (fibers) and the matrix by linear elastic compressible isotropic materials.

The results of the comparative analysis are the dependence of $|\varepsilon_{11}^{cr\,r}|$ on the geometrical parameter LD^{-1}. In the case of the infinite-fiber model, this quantity is the critical strain along the Ox_1-axis for both reinforcement and matrix. In the case of the finite-fiber model, we have

$$\varepsilon_{11}^{cr\,r} = \varepsilon_{11}^{cr\,r}(x_1, x_2) \quad \text{for} \quad x_1 = 0 \text{ and } x_2 = 0. \tag{2.20}$$

In this case, quantity (2.20) is the critical strain of the fiber along the Ox_1-axis at the middle of the fiber. The critical strain of the matrix along the Ox_1-axis determined at infinity can reach very different values. This situation should necessarily be taken into account when comparing results obtained using both models.

Figures 2.3 and 2.4 presents results for micro- and nanocomposites, respectively, with polymer matrix with the following mechanical parameters: $E_m = 2.68$ GPa, $\nu_m = 0.4$. For microcomposites, the following values of the mechanical and geometrical parameters were used: $E_r E_m^{-1} = 10, 30, 50, 100, 150$ (E_r and E_m are Young's moduli for the fibers and the matrix, respectively), $10 \le LD^{-1} \le 1510$. For nanocomposites, the following values of mechanical and geometrical parameters were used: $E_r E_m^{-1} = 285, 373, 448, 500, 1000, 10 \le LD^{-1} \le 2310$. The last two values of the parameter $E_r E_m^{-1}$ represent situations that

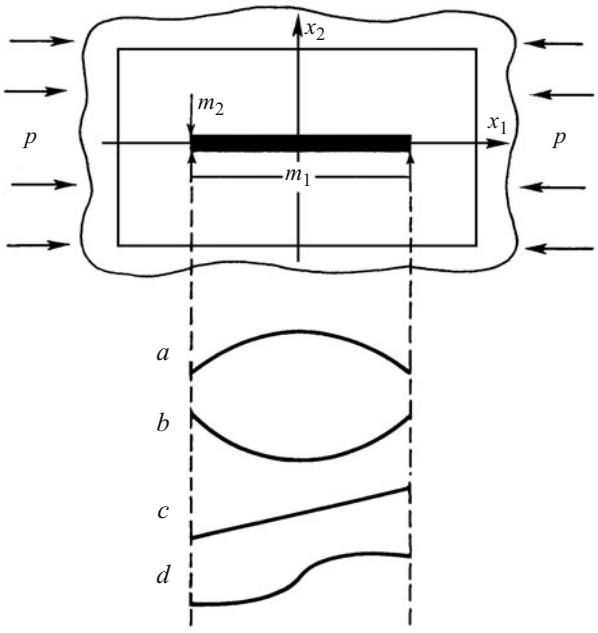

Fig. 2.5

may arise during the production of nanocomposites due to the strong dependence of the properties of the matrix on temperature. The solid lines correspond to the finite-fiber model, and the dashed lines to the infinite-fiber model.

It follows from Figs. 2.3 and 2.4 that for all values of $E_r E_m^{-1}$, as the geometrical parameter LD^{-1} increases within the specified range, the critical strains along the Ox_1-axis calculated using the finite-fiber model asymptotically tend to the critical strains obtained using the infinite-fiber model. The critical strains practically coincide for the upper values of the geometrical parameter. Thus, all the results for microcomposites and nanocomposites with polymer matrix obtained using the finite-fiber and infinite-fiber models are consistent.

Moreover, for relatively short fibers, there is a significant difference between the critical strains calculated using the finite-fiber and infinite-fiber models. For example, in the range $10 \le LD^{-1} \le 100$, the critical strains along the Ox_1-axis calculated using the infinite-fiber model are severalfold higher than the critical strains calculated using the long-fiber model. For the shortest fibers ($LD^{-1} = 10$), the critical strains along the Ox_1-axis calculated using the infinite-fiber model are almost an order of magnitude higher than the critical strains calculated using the long-fiber model. Thus, micro- and nanocomposites with $10 \le LD^{-1} \le 100$ are rather short fibers to which the infinite-fiber model is believed to be inapplicable.

This situation can be explained as follows: an analysis of the buckling modes of a fiber in a matrix (its results are detailed below) established that relatively short fibers buckle in modes that have nothing in common with periodic (along the fiber) buckling modes, which is characteristic for the infinite-fiber model and is determined by separating out periodic factors. For example, for relatively short and quite stiff fibers, the finite-fiber model predicted a buckling mode in which fibers turn as a perfectly rigid body. It is natural that such buckling modes are not described by the infinite-fiber model with isolated periodic factor. This is why the critical strains corresponding to this phenomenon cannot be calculated using the infinite-fiber model.

This completes the comparative analysis of results on stability of nanocomposites with polymer matrix obtained using the two models.

Remark 1. At first sight, the value $LD^{-1} = 100$, which is the upper limit of the range for which the infinite-fiber model is inapplicable, corresponds to quite long fibers. More details can be drawn from the scale of levels proposed in [12, 48]. According to this scale, the fiber diameter is $D \approx (10^{-4} - 10^{-8})$ m in microcomposites and $D \approx (10^{-7} - 10^{-9})$ m in nanocomposites. Thus, the infinite-fiber model is inapplicable to materials with linear dimensions along fibers that are equal to or less than those for microcomposites (1 cm – 1 μm) and nanocomposites (10 μm – 0.1 μm). Thus, the fiber lengths at which the infinite-fiber model is inapplicable are not great.

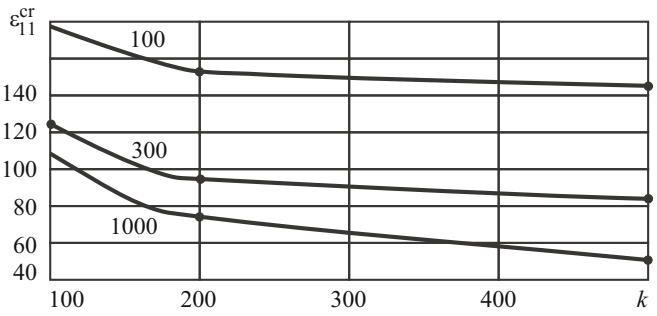

Fig. 2.6

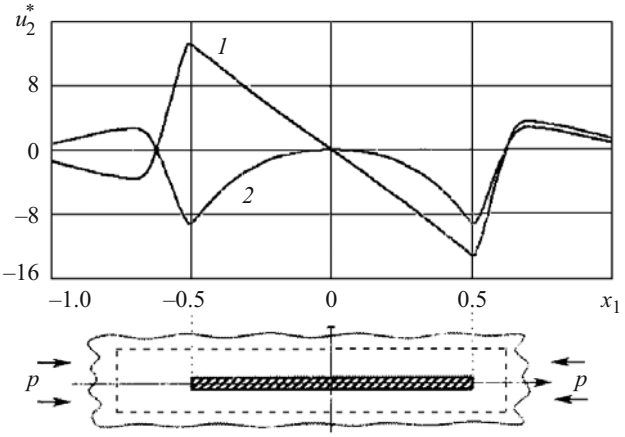

Fig. 2.7

Remark 2. It should be noted that the results of the comparative analysis of the infinite-fiber and finite-fiber models are strongly dependent on what quantities are compared. Such a quantity used here is the critical strain along a fiber for which expression (2.20) holds in the case of the finite-fiber model (Fig. 2.1) and the following expression holds in the case of the infinite-fiber model (Fig. 1.19):

$$\varepsilon_{11}^{0(\mathrm{r})} = \varepsilon_{11}^{0(\mathrm{m})} = \varepsilon_{11}^{0} = \mathrm{const}. \tag{2.21}$$

This choice is believed to be physically justified. The results would be absolutely different if the comparison quantity was the critical strain along the Ox_1-axis for the matrix at infinity. For the infinite-fiber model, comparison would be made for the same quantity, in view of (2.21). If the critical strain at infinity of the matrix was calculated using the finite-fiber model, much greater values would be obtained because the matrix is much less stiffer than the fibers.

It should be noted that the critical strain $|\varepsilon_{11}^{\mathrm{cr}}| = |\varepsilon_{11}^{\mathrm{cr\,m}}|^{\infty}$ at infinity of the matrix (Fig. 2.1) was used in [9–11, 14–18, 36–38, 48–54], where only the finite-fiber model was used:

$$|\varepsilon_{11}^{\mathrm{cr\,m}}|^{\infty} = |\varepsilon_{11}^{\mathrm{cr\,m}}| \quad \text{as} \quad x_1 \to \pm\infty. \tag{2.22}$$

In this connection (in contrast to Figs. 2.3 and 2.4), the value (2.22) appears much greater than $|\varepsilon_{11}^{\mathrm{cr\,r}}|$ and asymptotically tends from above to that obtained using the infinite-fiber model, as evidenced in [9, Fig. 3].

The considerations given in Remarks 1 and 2 should be taken into account in comparing the solutions of buckling problems for composites obtained using the infinite-fiber and finite-fiber models. More details on the comparative analysis of the models and their limits of applicability can be found in [48].

2.2. Analysis of Internal Instability. We will briefly discuss results on the internal instability of short-fiber reinforced composites under compression along the fibers obtained using the finite-fiber model. Numerical results obtained using this approach were analyzed, and the effect of mechanical and geometrical parameters on the critical strain of a composite and the buckling modes of the reinforcement were examined.

Remark. The distribution of stresses, strains, and displacements in buckling modes predicted by the finite-fiber model is complex; therefore, it is expedient to introduce quantities to describe these buckling modes. Here, such quantities are imaginary buckling modes that characterize the deformation pattern of the matrix and fibers during buckling and are the shape of the middle horizontal line of the fiber after buckling. Note that imaginary buckling modes are based on physical considerations and introduced to describe buckling modes when interpreting numerical solutions and are not used to solve problems.

2.2.1. One Fiber in a Matrix. The buckling of a composite under a compressive load along the fibers (axis Ox_1) was studied. The composite is under-reinforced with fibers of finite length and is in plane strain conditions provided by a constant load P acting at infinity (Fig. 2.5). Since the volume fraction of reinforcement is low, it is possible to neglect the interaction of

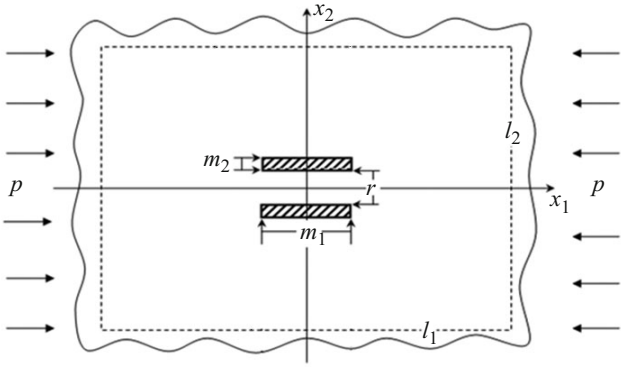

Fig. 2.8

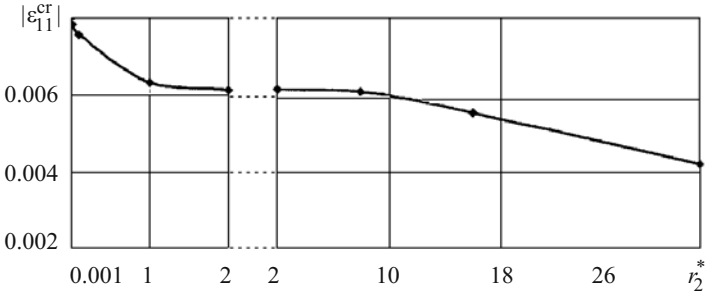

Fig. 2.9

neighboring fibers in both determining the subcritical state and studying buckling. Such problems may be considered as "model" or "reference" ones in the mechanics of composites.

Figures 2.5*a–d* show imaginary buckling modes symmetric about the middle of the fiber. The solid lines represent the horizontal middle line of the fiber after buckling. Buckling modes (Fig. 2.5*a*, *b*) can be called symmetric, while buckling modes (Fig. 2.5*c*, *d*) antisymmetric about the vertical axis Ox_2.

Symmetric buckling modes can be called flexural modes, similarly to the buckling mode of a strip under axial compression. The antisymmetric buckling mode corresponds to a rigid-body turn of a fiber when the matrix does not ensure adequate support because of which a kind of a plastic hinge forms near the fiber ends during buckling. It is obvious such a buckling mode can occur when the matrix and the reinforcement differ considerably in stiffness, which is typical of production processes for composites. The antisymmetric buckling mode (Fig. 2.5*d*) corresponds a turn of a fiber accompanied by bending.

The numerical solution of buckling problems are presented in Fig. 2.6 as the dependence of $|\varepsilon_{11}^{cr}|$ (2.22) (which is the critical strain along Ox_1-axis for the matrix at infinity) on the shape factor $k = m_1 m_2^{-1} = LD^{-1}$ of the fiber (length-to-diameter ratio).

The following mechanical and geometrical parameter values were used: $E_r E_m^{-1} = 100, 200, 300, 500, 1000$, $E_m = 2.76$ GPa, $\nu_m = \nu_r = 0.35$; $100 \le k < 500$.

It was established that all values of the critical strain is much less than 0.028, which corresponds to the ultimate strength of the matrix (cast polyamide). This suggests that a composite under-reinforced with fibers of finite length can undergo fracture due to microbuckling before the ultimate strength of the matrix is reached.

Let us now discuss some results on buckling modes. A buckling mode is characterized by the dimensionless displacement u_2 along the vertical axis divided by an amplitude factor:

$$u_2^*(x_1) = \left[u_2(x_1, x_2)\big|_{x_2=0} \right] \cdot \left[\left| \max\left\{ u_2(x_1, x_2)\big|_{x_2=0} \right\} \right| \right]^{-1}. \qquad (2.23)$$

For example, Fig. 2.7 shows buckling modes for $k = 10$ (curve *1*) and $k = 30$ (curve *2*).

It may be concluded that relatively short fibers buckle in a mode similar to the imaginary antisymmetric mode shown in Fig. 2.5*c*.

For $k \ge 30$ and constant values of the elastic moduli of the composite components, the reinforcement undergoes buckling in flexural mode (Fig. 2.5*a*).

More details on stability of composites under-reinforced with fibers of finite length (including the dependence of the critical strains on the mechanical and geometrical parameters of composites and possible buckling modes of the reinforcement) can be found in [9, 10, 52, 53].

2.2.2. Two Fibers along the Line of Action of a Compressive Load. Figure 2.8 represents a composite reinforced with fibers of finite length and low volume fraction that can interact with each other due to the irregularity of the internal structure. Let

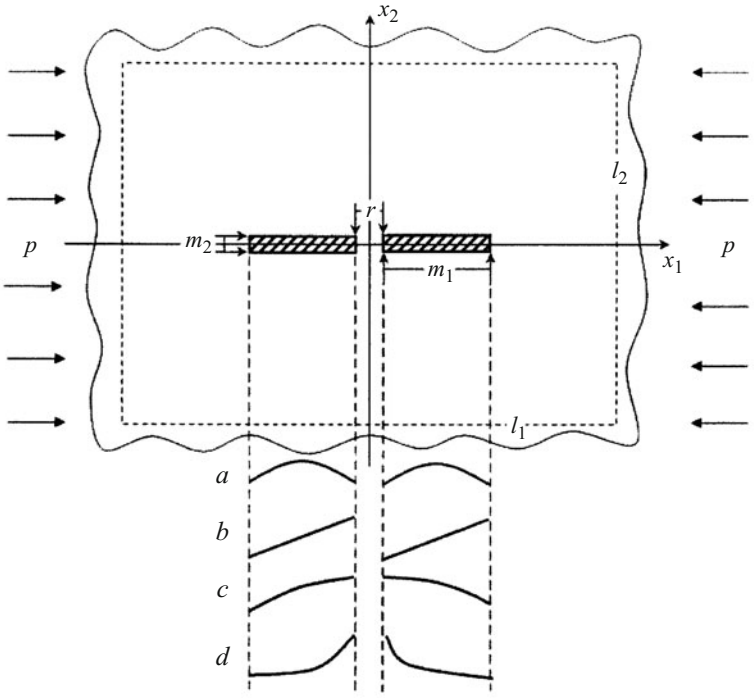

Fig. 2.10

us first consider two identical fibers of finite length aligned with the line of action of the compressive load and interacting with each other both in the subcritical state and during buckling. Plane strain in the plane x_1Ox_2 is assumed.

An additional parameter r is introduced to characterize the distance between neighboring parallel fibers. The corresponding dimensionless parameter $r_2^* = r \cdot m_1^{-1}$ (Fig. 2.8) is used to present the results.

To obtain specific results for two parallel fibers of finite length, computational experiments were conducted to identify an external rectangle $l_1 \times l_2$ such that it includes two parallel fibers and the conditions of decay on its boundary are satisfied.

Figure 2.9 shows the dependence of the critical strain $|\varepsilon_{11}^{\mathrm{cr}}|$ along the Ox_1-axis for the matrix at infinity on the relative distance r_2^* between the fibers. The following mechanical and geometrical parameters of the composite components were used: $E_{\mathrm{r}} E_{\mathrm{m}}^{-1} = 1000, \nu_{\mathrm{r}} = \nu_{\mathrm{m}}; k = m_1 / m_2 = 100, 0.001 \le r_2^* \le 32$.

Note that situations in which the critical strain $|\varepsilon_{11}^{\mathrm{cr}}|$ decreases and the dimensionless parameter r_2^* increases from $r_2^* \approx 0.001$ to $r_2^* \approx 2$ are typical for engineering. For example, when $r_2^* \approx 0.001$, the fibers almost touch each other and deform as a single fiber of the same length and double diameter during buckling. As the distance between the fibers is increased to $r_2^* \approx 2$, they tend to deform independently during buckling. Thus, as the parameter r_2^* is increased, the parameter k for one fiber as if increases too, and, similarly to Fig. 2.6 for one fiber, as the parameter k increases, the critical strain $|\varepsilon_{11}^{\mathrm{cr}}|$ along the Ox_1-axis decreased.

Figure 2.10 represents a composite reinforced with fibers of finite length and low volume fraction such that two neighboring inline fibers aligned with the line of action of the compressive load can interact with each other due to the irregularity of the internal structure either in the subcritical state or during buckling. Plane strain in the plane x_1Ox_2 is assumed.

Similarly to the situation with one fiber in Fig. 2.10, four buckling modes can be imagined for two inline fibers. These imaginary modes are shown by solid lines in Fig. 2.10*a–d*, which represent the middle lines of the fibers after buckling.

The flexural buckling mode (Fig. 2.10*a*) corresponds to the case where the fibers buckle almost independently of each other. The buckling mode (Fig. 2.10*b*) is an almost rigid-body turn of each fiber. This is possible when the fibers are rather stiff and the matrix does not provide the appropriate support, which results in the formation of a kind of plastic hinge at the fiber ends during buckling. The buckling mode (Fig. 2.10*c*) corresponds to the case where the two fibers buckle in the same flexural mode.

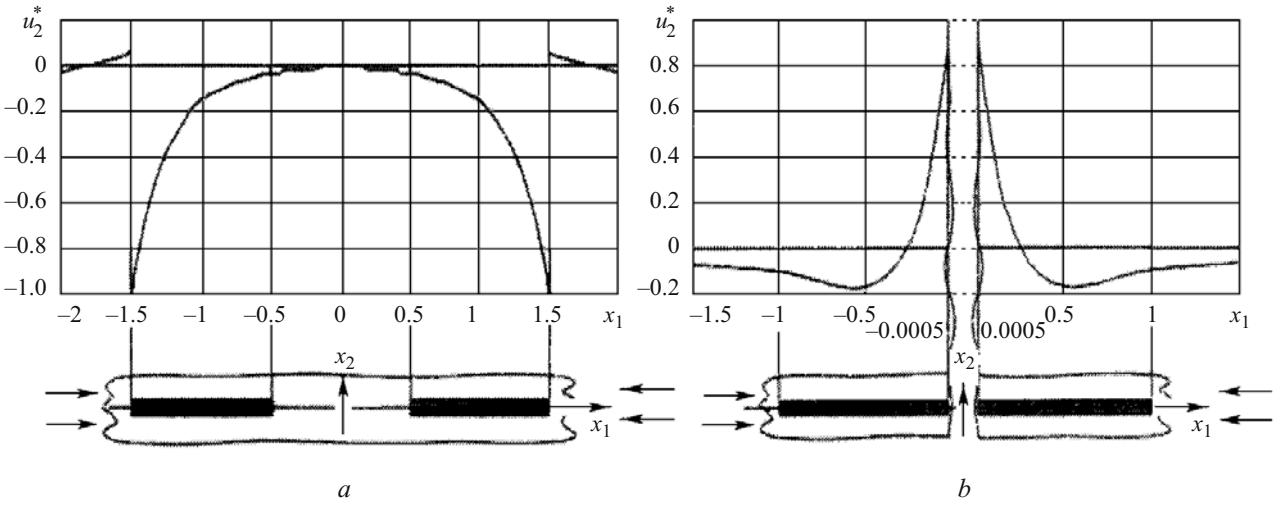

a *b*

Fig. 2.11

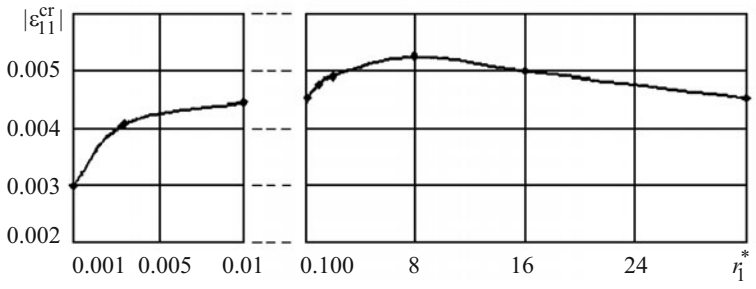

Fig. 2.12

The buckling mode (Fig. 2.10*d*) corresponds to the case where the two fibers undergo relatively rigid turn and bending. This is possible when the fibers are rather stiff and the matrix does not provide the appropriate support, which results in the formation of a kind of plastic hinge between the fibers ends during buckling. The construction of imaginary modes can be continued considering the buckling modes in Fig. 2.10*a–d* as the first imaginary modes.

It should be noted that the first imaginary buckling modes in Fig. 2.10*a–d* for two inline fibers of finite length and in Fig. 2.5*a–d* for one fiber of finite length are constructed before the numerical solution of buckling problems only to analyze the numerical results obtained.

To obtain specific results for two inline fibers of finite length, computational experiments were conducted to identify an external rectangle $l_1 \times l_2$ such that it includes two inline fibers and the conditions of decay on its boundary are satisfied. Also, computational experiments were conducted to choose a nonuniform mesh spacing in the region of contact between the composite components.

Additionally, a dimensionless parameter r_1^* characterizing the relative distance between two neighboring inline fibers is introduced as $r_1^* = r \cdot m_1^{-1}$ (Fig. 2.10). The following mechanical and geometrical parameters of the composite components were used: $E_r E_m^{-1} = 1000, \nu_r = \nu_m; k = m_1 / m_2 = 100, 0.001 \le r_1^* \le 32$.

Figure 2.11 shows the variation of the dimensionless displacement (2.23) along the Ox_1-axis for $r_1^* = 1$ (Fig. 2.11*a*; the distance between the ends of the fibers equals the fiber length) and $r_1^* = 0.001$ (Fig. 2.11*b*).

Thus, when $r_1^* = 1$, buckling occurs in a mode similar to the imaginary buckling mode in Fig. 2.10*c* as a general flexural mode. When $r_1^* = 0.001$, buckling occurs in a mode similar to the imaginary mode in Fig. 2.10*d* as mutual turn and bending in the presence of a hinge between the fiber ends.

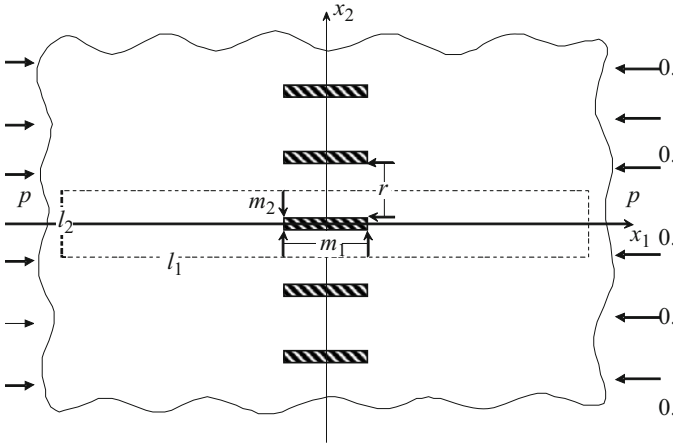

Fig. 2.13

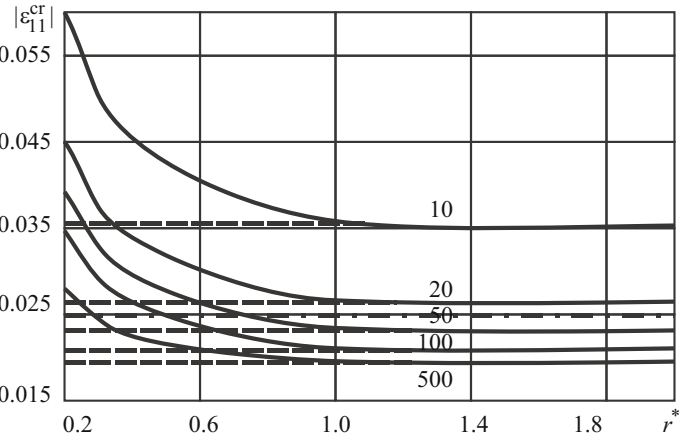

Fig. 2.14

The results of studying the influence of the interaction of two inline fibers of finite length on the critical strain are presented in Fig. 2.12, which shows the dependence of the critical strain $|\varepsilon_{11}^{cr}|$ along the Ox_1-axis on the relative distance r_1^* between the cylinder ends, the range of r_1^* being divided into two parts ($0.001 \le r_1^* \le 0.01$ and $0.1 \le r_1^* \le 32$) with different scales for the Or_1^*-axis.

It may be concluded that when the distance between the fibers of finite length is quite long ($r_1^* > 30$), the critical strain $|\varepsilon_{11}^{cr}|$ tends to the value corresponding to the case of one fiber in a matrix and the buckling mode is similar to the imaginary mode in which each fiber buckles almost without interaction with the other fiber (Fig. 2.10*a*). With decrease in r_1^*, the interaction of the fibers becomes stronger. For example, the general flexural mode (Fig. 2.10*c*) occurs and $|\varepsilon_{11}^{cr}|$ reaches the maximum when $0.005 \le r_1^* \le 30$ and $r_1^* = 8$ and the mutual turn and bending of the fibers occurs in the presence of a hinge between their ends (Fig. 2.10*d*) and the critical strain $|\varepsilon_{11}^{cr}|$ sharply decreases when $0.001 \le r_1^* \le 0.005$.

Thus, the numerical analysis revealed that the critical strain depends nonmonotonically on the distance between the ends of inline fibers. This mechanical effect was discovered for the first time in the cited publication. The effect may be explained by the fact that the buckling modes change in the range of distances between the ends of inline fibers under consideration.

More details on the stability of composites reinforced with interacting fibers of finite length can be found in [11, 14, 15, 49, 54].

2.2.3. Periodic Row of Fibers along the Line of Action of a Compressive Load. Let us consider a composite reinforced with identical fibers of finite length regularly arranged in periodic rows and interacting with each other which each row. The rows of fibers are parallel and spaced so far that fibers in different rows do not interact either in the subcritical state nor during buckling.

Figure 2.13 represents composites in which the volume fraction of fibers is such that one can analyze only one periodic (along the Ox_2-axis) row of parallel identical fibers of finite length that interact with each other (within a row) either in the subcritical state or during buckling. A parameter r characterizing the distance between neighboring parallel fibers is additionally introduced. The dimensionless parameter $r^* = r \cdot m_1^{-1}$ (Fig. 2.13) can also be used to present the results.

An external rectangle $l_1 \times l_2$ is chosen by way of computational experiments so that the results are independent of $l_1 \times l_2$. In the case of a periodic (along the Ox_2-axis) row of identical fibers, the side length l_2 of the rectangle along the Ox_2-axis is selected from the periodicity condition. If the buckling mode along the Ox_2-axis has period equal to the period of structure, then $l_2 = m_2 + r$, where the period of structure on the right-hand side is denoted as in Fig. 2.13. The external rectangle $l_1 \times l_2$ is shown in Fig. 2.13 by a dashed line, and only the value of l_1 is determined in a computational experiment.

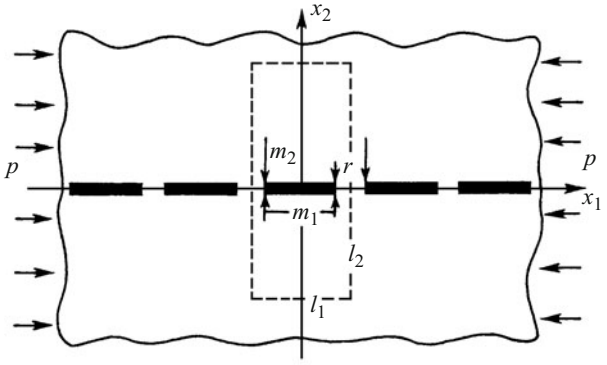

Fig. 2.15

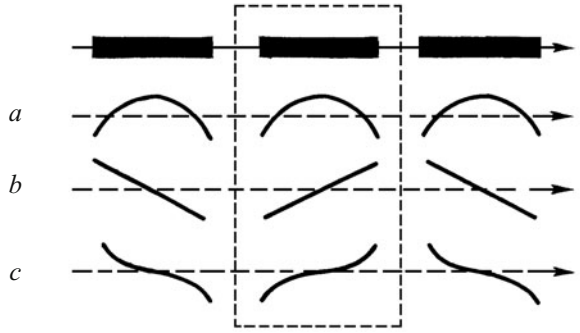

Fig. 2.16

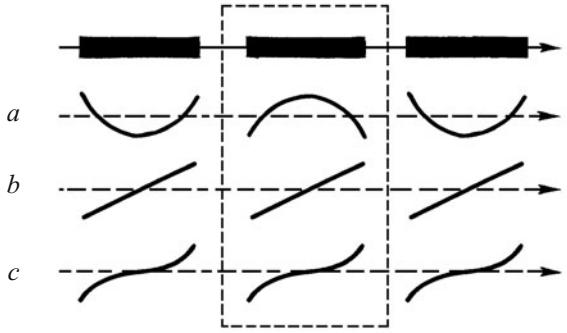

Fig. 2.17

If the structure is periodic (Fig. 2.13) with period $T = m_2 + r$, it is possible to consider buckling modes along the Ox_2-axis with period multiple of the structure period $N(m_2 + r)$, where N is an integer. In this case, the size $N(m_2 + r)$ of the external rectangle $l_1 \times l_2$ can be found from the expression $l_2 = N(m_2 + r)$.

Figure 2.14 shows the dependence of the critical strain $|\varepsilon_{11}^{\mathrm{cr}}|$ along the Ox_1-axis at infinity on the relative distance r^* between neighboring fibers within one periodic row. The following mechanical and geometrical parameters of the composite components were used: $E_{\mathrm{r}} E_{\mathrm{m}}^{-1} = 500$, $\nu_{\mathrm{r}} = \nu_{\mathrm{m}}$, $k = m_1 / m_2 = 10, 20, 50, 100, 500$; $0.02 \le r^* \le 5$.

From Fig. 2.14, it may be concluded that as the distance between neighboring fibers exceeds the fiber length ($r^* > 1$), the critical strain periodic along the Ox_2-axis of a row of parallel fibers of finite length hardly changes and tends to the values obtained for one fiber in a matrix and shown by dashed lines in Fig. 2.14. As the distance between neighboring fibers in a row of parallel fibers decreases ($r^* < 1$), the critical strain increases.

Figure 2.15 represents composites in which the volume fraction of fibers is such that one can analyze only one periodic (along the Ox_1-axis) row of inline identical fibers of finite length that interact with each other (within a row) either in the subcritical state or during buckling.

A parameter r characterizing the distance between neighboring parallel fibers is additionally introduced. The dimensionless parameter $r^* = r \cdot m_1^{-1}$ (Fig. 2.15) can also be used to present the results.

An external rectangle $l_1 \times l_2$ is chosen by way of a computational experiment so that the results are independent of $l_1 \times l_2$. In the case of a periodic (along the Ox_1-axis) row of identical fibers, the side length l_1 of the rectangle along the Ox_1-axis is selected from the periodicity condition. If the buckling mode along the Ox_1-axis has period equal to the period of structure, then $l_1 = m_1 + r$, where the period of structure on the right-hand side is denoted as in Fig. 2.15. The external rectangle $l_1 \times l_2$ is shown in Fig. 2.15 by a dashed line, and only the value of l_2 is determined in a computational experiment.

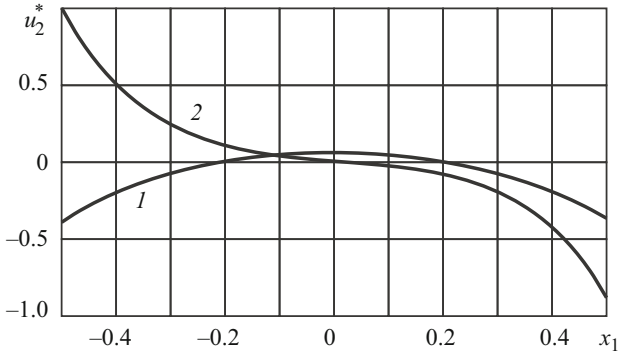

Fig. 2.18

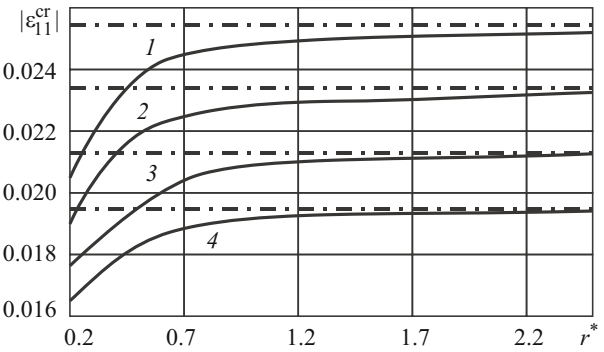

Fig. 2.19

If the structure is periodic (Fig. 2.15) with period $T = m_1 + r$, it is possible to consider buckling modes along the Ox_1-axis with period multiple of the structure period $N(m_1 + r)$, where N is an integer. In this case, the size $N(m_1 + r)$ of the external rectangle $l_1 \times l_2$ can be found from the expression $l_1 = N(m_1 + r)$.

By analogy with one and two inline fibers, it makes sense to analyze imaginary buckling modes for a periodic row of inline fibers of finite length. Figures 2.16*a–c* and 2.17*a–c* show imaginary buckling modes that are, respectively, symmetric and antisymmetric about the vertical lines drawn through the middle points between the ends of neighboring fibers. The buckling modes in Figs. 2.16*a* and 2.17*b*, *c* are periodic along the Ox_1-axis with period equal to the structure period T, and the buckling modes in Figs. 2.16*b*, *c* and Fig. 2.17*a* are periodic along the Ox_1-axis with period equal to $2T$.

The buckling mode in Fig. 2.16*a* can be considered similar to the flexural mode for far spaced, noninteracting fibers. The buckling mode in Fig. 2.16*b* can be considered similar to the rigid-body turn of closely spaced fibers that are stiffer than the matrix so that it does not provide appropriate support, resulting in a plastic hinge between the fiber ends. The buckling mode in Fig. 2.16*c* can be considered similar to the turn and bending of relatively stiff fibers (this mode may be considered to result from imposing bending on the fibers in Fig. 2.16*b*). It is convenient to use these considerations on imaginary buckling modes when describing buckling modes obtained numerically.

To analyze buckling modes, Fig. 2.18 shows the variation of the dimensionless displacement (2.23) along the Ox_1-axis for $r^* = 1$ (curve *1*) and $r^* = 0.2$ (curve *2*).

Buckling mode *1* in Fig. 2.18 is very similar to the flexural modes in Figs. 2.16*a* and 2.17*a* for noninteracting fibers (one isolated fiber in a matrix). Buckling mode *2* in Fig. 2.18 is very similar to the modes (turn and bending) in Figs. 2.16*c* and 2.17*c*. Thus, as inline fibers within a periodic row draw close to each other, buckling modes change. The situation with two inline fibers is similar.

Figure 2.19 shows the critical strain $|\varepsilon_{11}^{cr}|$ versus the relative distance r^* between neighboring fibers for the following mechanical and geometrical parameters: $E_r E_m^{-1} = 1000$, $\nu_r = \nu_m$, $k = m_1 / m_2$ = 100, 200, 300, 500 (curves *1*, *2*, *3*, *4*, respectively); $0.2 \le r^* \le 4.5$ (the dash-and-dot lines represent the values of $|\varepsilon_{11}^{cr}|$ for one fiber at the same values of k).

It can now be concluded that if the distance between neighboring fibers exceeds the fiber length ($r^* > 1$), the critical strain $|\varepsilon_{11}^{cr}|$ for a periodic row of inline fibers of finite length is practically equal to $|\varepsilon_{11}^{cr}|$ for one isolated fiber of finite length in a matrix (dashed lines).

More details on the stability of composites reinforced with periodic rows of interacting fibers of finite length can be found in [16, 17, 36, 37, 50].

2.3. Analysis of Near-Surface Instability. Here we will briefly discuss results on the stability of composites under-reinforced with short fibers near the free plane boundary and compressed along fibers parallel to the boundary (Fig. 2.20).

Since the volume fraction of the reinforcement is low, the interaction between fibers is neglected; therefore, a composite in plane strain conditions is modeled in Cartesian coordinates $x_1 Ox_2$ by a semi-infinite matrix reinforced with one short fiber along the Ox_1-axis coinciding with the free boundary.

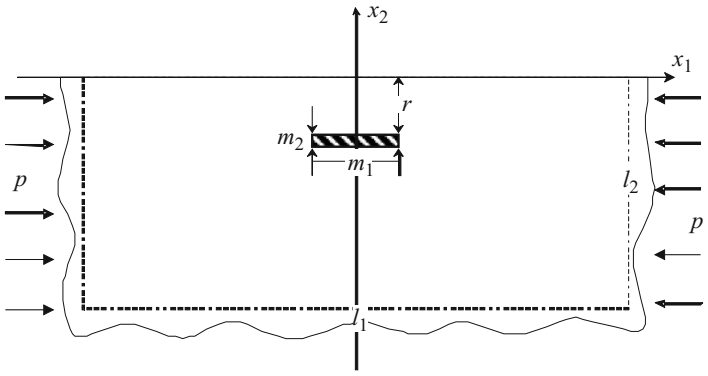

Fig. 2.20

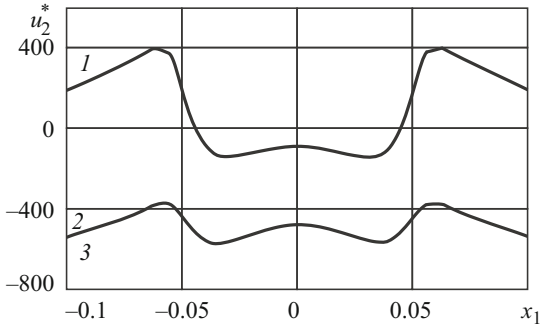

Fig. 2.21

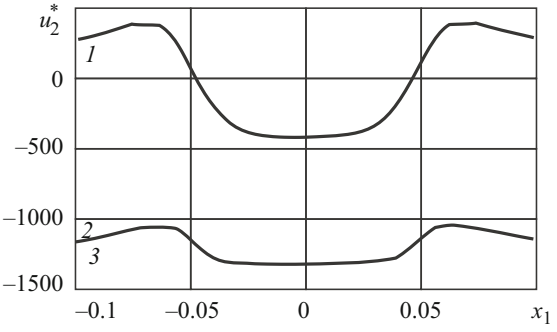

Fig. 2.22

2.3.1. Specific Features of Near-Surface Instability. An analysis of the subcritical stress–strain state of the composite revealed that a compressive load induces an asymmetric subcritical state that causes initial curving of the short fiber near the free boundary.

Let us first discuss some results from the analysis of the subcritical stress–strain state for the following mechanical and geometrical parameters: $E^* = E_r E_m^{-1} = 343, \nu_1 = \nu_2 = 0.4, LD^{-1} = m_1 / m_2 = 1000, 0 \le r^* = r / m_1 \le 15$.

To analyze the initial shape mode of the fiber, we will consider the variation of the vertical displacements $u_2(x_1)$ along the Ox_1-axis in the range $x_1 = \pm m_1$ (where $x_1 = \pm m_1 / 2$ corresponds to the fiber) for the lines $x_2 = r + m_2 / 2, r + m_2, r$ that pass through the horizontal axis of the fiber and the lower and upper contact lines of the composite components for $r^* = 0$.

If the distance from the fiber is quite great ($r^* = 15$), the distribution of displacements of the fiber about its axis is symmetric and the fiber axis is straight. In this case, the fiber that is on the surface ($r^* = 0$) curves together with the boundary surface toward the region not filled with matrix material. It is obvious that the asymmetry of the initial stress–strain state is due to the interaction between the fiber and the free boundary under the compressive load.

Let us analyze the dependence of the curvature of the fiber on the distance to the boundary r^*. Figures 2.21 and 2.22 show the variation of the vertical displacements $u_2(x_1)$ in the range $x_1 = \pm m_1$ for the lines $x_2 = r, r + m_2 / 2$ (curves *2* and *3*) that pass through the horizontal axis of the fiber and the upper contact of the composite components that is closer to the boundary and the boundary line $x_2 = 0$ (curve *1*) for $r^* = 0.1$ and $r^* = 0.2$, respectively.

From these results it follows that as the distance between the fiber and the boundary increases, the direction of bending of the fiber changes. For example, Fig. 2.23 shows the dependence of the displacement $u_2^* = u_2^0\big|_{x_1=0} - u_2^0\big|_{x_1=m_1/2}$ of the fiber's center of symmetry $x_2 = r + m_2 / 2$ about the ends (curve *1*) and its projection $x_2 = 0$ onto the boundary surface (curve *2*) on the distance r^*.

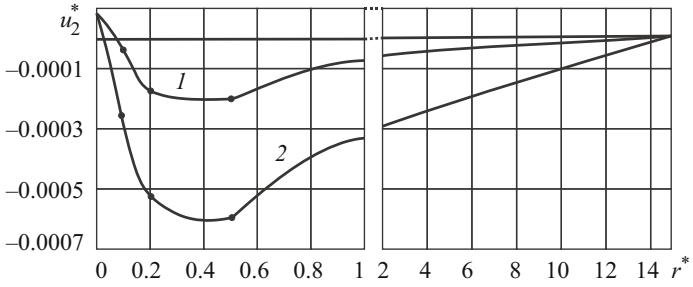

Fig. 2.23

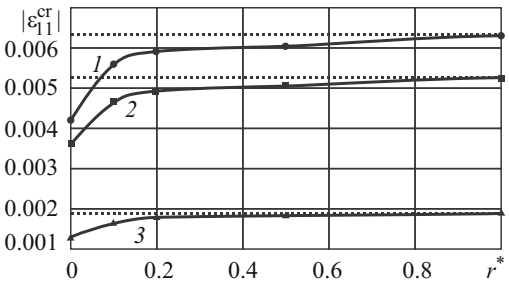

Fig. 2.24

It can be seen that for $r^* = 0$ (the fiber is on the surface), the middle line of the fiber shifts toward the region not filled with matrix material, while the fiber ends remain in the matrix. With distance from the surface, the matrix material that is between the fiber and the boundary as if presses the fiber into the matrix, and only at rather long distances ($r^* > 15$), the fiber and the boundary do not affect each other.

2.3.2. Analysis of Numerical Solutions of the Buckling Problem. To solve the problems posed, we isolate in the semi-infinite matrix a rectangular domain containing reinforcement and having one side on the free boundary. The dimensions l_i of the domain are determined in computational experiment so that the conditions of decay of the perturbations caused by the stress concentration around the fiber are satisfied on the sides of the rectangle that do not coincide with the boundary.

The following mechanical and geometrical parameters of the composite components were used: $E^* = E_r E_m = 343$, $1000, \nu_r = \nu_m, k = m_1 / m_2 = 200, 1000, 0 \le r^* = r / m_1 \le 15$. Figure 2.24 shows the dependence of the absolute critical strain ε_{11}^{cr} on the dimensionless distance r^* between the fiber and the boundary for $E^* = 1000, k = 1000$ (curve *1*); $E^* = 343, LD^{-1} = 200$ (curve *2*); $E^* = 1000, LD^{-1} = 200$ (curve *3*). The dashed lines represent the case of one fiber in a matrix with the same mechanical and geometrical parameters.

The above results on the stability of a composite under-reinforced with short fibers near the free plane boundary allow us to conclude whether buckling is possible under compression along fibers parallel to the boundary. If the distance between the fiber and the boundary exceeds the fiber length, internal instability occurs. With decrease in this distance, near-surface instability occurs.

More results on the stability of composites under-reinforced with fibers of finite length near the free plane boundary can be found in [18, 38].

2.4. Conclusions to Sec. 2. In Sec. 2, we have discussed results on microbuckling in compressed composites obtained using the finite-fiber model. The following conclusions can now be made.

When applied to the analysis of the stability of composites reinforced with short fibers, the finite-fiber model allows describing reinforcements of finite dimensions. The results obtained using the finite- and infinite-fiber models have appeared consistent.

By analyzing the solutions of buckling problems for one fiber, two fibers of finite length, periodic rows of identical fibers, and a short fiber near the free boundary, we have studied the influence of the mechanical and geometrical parameters of the composite components on the critical strain and the buckling mode of interacting fibers. New mechanical effects have been revealed.

One relatively short fiber undergoes a rigid-body turn when the matrix does not provide sufficient support and a plastic hinge occurs near the fiber ends.

Two inline fibers of finite length either buckle in one flexural mode or turn and bend when the matrix between the fibers does not provide sufficient support and a plastic hinge occurs between the fibers.

The dependence of the critical strain for two inline fibers of finite length on the distance between the fiber ends is nonmonotonic, which is due to the change of buckling modes at a certain distance between the fibers.

By comparing results obtained using the infinite- and finite-fiber models, we have validated the former results and have established the following limits of applicability of these models:

– in the range $10 \le LD^{-1} \le 100$, the critical strains along the Ox_1-axis calculated using the infinite-fiber model are severalfold higher than the critical strains calculated using the long-fiber model;

– for the shortest fibers ($LD^{-1} = 10$), the critical strains along the Ox_1-axis calculated using the infinite-fiber model are almost an order of magnitude higher than the critical strains calculated using the long-fiber model.

Thus, the infinite-fiber model is inapplicable in the range $10 \le LD^{-1} \le 100$. Hence, fibers with $LD^{-1} = 100$ are considered quite short, and the infinite-fiber model cannot be used.

REFERENCES

1. A. Ya. Gol'dman, N. F. Savel'eva, and V. I. Smirnov, "Mechanical properties of glass fabric-reinforced plastics in tension and compression normal to the plane of reinforcement," *Mech. Comp. Mater.*, **4**, No. 4, 643–648 (1968).
2. A. N. Guz, "On setting up a stability theory of unidirectional fibrous materials," *Int. Appl. Mech.*, **5**, No. 2, 156–162 (1969).
3. A. N. Guz, "Determining the theoretical compressive strength of reinforced materials," *Dokl. AN USSR*, *Ser. A*, No. 3, 236–238 (1969).
4. A. N. Guz, *Stability of Three-Dimensional Deformable Bodies* [in Russian], Naukova Dumka, Kyiv (1971).
5. A. N. Guz, *Stability of Elastic Bodies Subject to Finite Deformations* [in Russian], Naukova Dumka, Kyiv (1973).
6. A. N. Guz, *Fundamentals of the Three-Dimensional Theory of Stability of Deformable Bodies* [in Russian], Vyshcha Shkola, Kyiv (1986).
7. A. N. Guz, *Fracture Mechanics of Compressed Composite Materials* [in Russian], Naukova Dumka, Kyiv (1990).
8. A. N. Guz, *Fundamentals of the Fracture Mechanics of Compressed Composites* [in Russian], in 2 vols., Litera, Kyiv (2008).
9. A. N. Guz, V. A. Dekret, and Yu. V. Kokhanenko, "Plane problems of stability of composite materials with a finite-size filler," *Mech. Comp. Mater.*, **36**, No. 1, 49–54 (2000).
10. A. N. Guz, V. A. Dekret, and Yu. V. Kokhanenko, "Stability of composites with reinforcement of finite size in plane strain conditions," *Izv. Vuzov* (*Severokavkaz. Region*), Special issue, 60–63 (2001).
11. A. N. Guz, V. A. Dekret, and Yu. V. Kokhanenko, "Interaction of short fibers in a matrix during loss of stability: Plane problem," in: *Problems of Mechanics* [in Russian], Fizmatlit, Moscow (2003), pp. 331–341.
12. A. N. Guz, J. J. Rushchitsky, and I. A. Guz, *Introduction to the Mechanics of Nanocomposites* [in Russian], Akademperiodika, Kyiv (2010).
13. A. N. Guz, M. A. Cherevko, G. G. Margolin, and I. M. Romashko, "Failure of unidirectional boron-reinforced aluminum composites in compression," *Mech. Comp. Mater.*, **22**, No. 2, 158–162 (1986).
14. V. A. Dekret, "Solving the plane buckling problem for a composite reinforced with two short fibers," *Dop. NANU*, No. 8, 37–40 (2003).
15. V. A. Dekret, "Plane buckling problem for a composite reinforced with two parallel short fibers," *Dop. NANU*, No. 12, 38–41 (2003).
16. V. A. Dekret, "Stability of a composite reinforced with a periodic row of inline short fibers," *Dop. NANU*, No. 11, 47–50 (2004).
17. V. A. Dekret, "Stability of a composite reinforced with a periodic row of parallel short fibers," *Dop. NANU*, No. 12, 41–44 (2004).
18. V. A. Dekret, "Stability of a composite under-reinforced with short fibers near the free surface," *Dop. NANU*, No. 10, 49–51 (2006).
19. L. J. Broutman and R. H. Krock (eds.), *Composite Materials*, in 8 vols., Academic Press, New York–London (1974–1975).
20. A. Lawley and M. J. Koczak, "Role of the interface on elastic-plastic composite behavior," in: A. G. Metcalfe (ed.), *Interfaces in Metal Matrix Composites*, Vol. 1 of the eight-volume series *Composite Materials*, Academic Press, New York (1974), p. 212.
21. Yu. M. Tarnopol'skii (ed.), *Methods for Static Testing of Reinforced Plastics* [in Russian], Zinatne, Riga (1972).

22. V. V. Panasyuk (ed.), *Fracture Mechanics and Structural Strength: Handbook* [in Russian], in 4 vols., Kyiv, Naukova Dumka (1988–1990).
23. A. N. Guz (ed.), *Mechanics of Composite Materials* [in Russian], in 12 vols, Naukova Dumka (Vols. 1–4), A.S.K. (Vols. 5–12), Kyiv (1993–2003).
24. H. S. Katz and J. V. Milevski, *Handbook of Fillers and Reinforcements for Plastics* [Russian translation], Khimiya, Moscow (1981).
25. H. Liebowitz (ed.), *Fracture. An Advanced Treatise*, in 7 vols., Academic Press, New York–London (1968–1975).
26. B. W. Rosen, "Mechanics of composite strengthening," in: *Fiber Composite Materials*, *American Society of Metals*, Metals Park, Ohio (1965), pp. 37–75.
27. B. W. Rosen and N. F. Dow, "Mechanics of failure of fibrous composites," in: H. Liebowitz (ed.), *Fracture*, *An Advanced Treatise*, Vol. 7, Academic Press, New York (1972), pp. 612–672.
28. C. C. Chamis, "Microscopic strength theories," in: L. J. Broutman (ed.), *Fracture and Fatigue*, Vol. 5 of the eight-volume series *Composite Materials*, Academic Press, New York (1974), pp. 93–151.
29. G. P. Cherepanov, *Fracture Mechanics of Composite Materials* [in Russian], Nauka, Moscow (1983).
30. I. Yu. Babich and A. N. Guz, "Deformation instability of laminated materials," *Sov. Appl. Mech.*, **5**, No. 5, 488–491 (1969).
31. H. Budiansky, "Micromechanics," *Compos. Struct.*, **16**, No. 1, 3–13 (1983).
32. H. Budiansky and N. A. Fleck, "Compressive failure of fibre composites," *J. Mech. Phys. Solids*, **41**, No. 1, 183–211 (1993).
33. H. Budiansky and N. A. Fleck, "Compressive kinking of fibre composites: a topical review," *Appl. Mech. Rev.*, **47**, No. 6, Pt. 2, 246–250 (1994).
34. A. Kelly and C. Zweben, *Comprehensive Composite Materials*, in 6 vols., Elsevier (2006).
35. Ian Milne, R. O. Ritchie, and B. Karihaloo, *Comprehensive Structural Integrity*, in 10 vols., Elsevier (2006).
36. V. A. Dekret, "Two-dimensional buckling problem for a composite reinforced with a periodic row of collinear short fibers," *Int. Appl. Mech.*, **42**, No. 6, 684–691 (2006).
37. V. A. Dekret, "Plane stability problem for a composite reinforced with a periodic row of parallel fibers," *Int. Appl. Mech.*, **44**, No. 5, 498–504 (2008).
38. V. A. Dekret, "Near-surface instability of composites weakly reinforced with short fibers," *Int. Appl. Mech.*, **44**, No. 6, 619–625 (2008).
39. N. F. Dow and I. J. Gruntfest, "Determination of most needed potentially possible improvements in materials for ballistic and space vehicles," *General Electric Co.*, *Space Sci. Lab.*, *TIRS 60 SD 389*, June (1960).
40. N. A. Fleck, "Compressive failure of fiber composites," in: *Advances in Applied Mechanics*, Vol. 33, Academic Press, New York (1997), pp. 43–119.
41. A. N. Guz, "Mechanics of composite-material failure under axial compression (brittle failure)," *Sov. Appl. Mech.*, **18**, No. 10, 863–872 (1982).
42. A. N. Guz, "Stability theory for unidirectional fiber-reinforced composites," *Int. Appl. Mech.*, **32**, No. 8, 577–586 (1996).
43. A. N. Guz, *Fundamentals of the Three-Dimensional Theory of Stability of Deformable Bodies*, Springer-Verlag, Berlin (1999).
44. A. N. Guz, "On one two-level model in the mesomechanics of compression fracture of cracked composites," *Int. Appl. Mech.*, **39**, No. 3, 274–285 (2003).
45. A. N. Guz, "Establishing the foundations of the mechanics of fracture of materials compressed along cracks (review)," *Int. Appl. Mech.*, **50**, No. 1, 1–57 (2014).
46. A. N. Guz and I. A. Guz, "On the theory of stability of laminated composites," *Int. Appl. Mech.*, **35**, No. 4, 323–329 (1999).
47. A. N. Guz and I. A. Guz, "On models in the theory of stability of multi-walled carbon nanotubes," *Int. Appl. Mech.*, **40**, No. 1, 1–29 (2006).
48. A. N. Guz and V. A. Dekret, "On two models in the three-dimensional theory of stability of composites," *Int. Appl. Mech.*, **44**, No. 8, 839–854 (2008).

49. A. N. Guz and V. A. Dekret, "Interaction of two parallel short fibers in the matrix at loss of stability," *Computer Modeling in Engineering & Sciences*, **13**, No. 3, 165–170 (2006).
50. A. N. Guz and V. A. Dekret, "Stability problem of composite material reinforced by periodical row of short fibers," *Computer Modeling in Engineering & Sciences*, **42**, No. 3, 177–186 (2009).
51. A. N. Guz and V. A. Dekret, "Stability loss in nanotube reinforced composites," *Computer Modeling in Engineering & Sciences*, **49**, No. 1, 69–80 (2009).
52. A. N. Guz, V. A. Dekret, and Yu. V. Kokhanenko, "Solution of plane problems of the three-dimensional stability of a ribbon-reinforced composite," *Int. Appl. Mech.*, **36**, No. 10, 1317–1328 (2000).
53. A. N. Guz, V. A. Dekret, and Yu. V. Kokhanenko, "Planar stability problem of composite weakly reinforced by short fibers," *Mech. Comp. Mater. Struct.*, No. 12, 313–317 (2005).
54. A. N. Guz, V. A. Dekret, and Yu. V. Kokhanenko, "Two-dimensional stability problem for interacting short fibers in a composite: In-line arrangement," *Int. Appl. Mech.*, **40**, No. 9, 994–1001 (2004).
55. A. N. Guz, Yu. N. Lapusta, and A. N. Samborskaya, "A micromechanics solutions of a 3D internal instability problem for a fiber series on an infinite matrix," *Int. J. Fracture*, **116**, No. 3, L55–L60 (2002).
56. A. N. Guz, Yu. N. Lapusta, and A. N. Samborskaya, "3D model and estimation of fiber interaction effects during internal instability in non-linear composites," *Int. J. Fracture*, **134**, No. 3–4, L45–L51 (2005).
57. A. N. Guz, A. A. Kritsuk, and R. F. Emel'yanov, "Character of the failure of unidirectional glass-reinforced plastic in compression," *Sov. Appl. Mech.*, **5**, No. 9, 997–999 (1969).
58. A. N. Guz and A. N. Samborskaya, "General stability problem of a series of fibers in an elastic matrix," *Sov. Appl. Mech.*, **27**, No. 3, 223–230 (1991).
59. H. Katz and J. V. Milevski (eds.), *Handbook of Fillers and Reinforcements for Plastics*, Van Nostrand Reinhold Company, New York (1978).
60. Ch. Jochum and J.-C. Grandidier, "Microbuckling elastic modeling approach of a single carbon fiber embedded in an epoxy matrix," *Compos. Sci. Techn.*, **64**, 2441–2449 (2004).
61. A. A. Kaminsky, "Mechanics of the delayed fracture of viscoelastic bodies with cracks: Theory and experiment (review)," *Int. Appl. Mech.*, **50**, No. 5, 485–548 (2014).
62. L. P. Khoroshun and L. V. Nazarenko, "Deformation and damage of composites with anisotropic components (review)," *Int. Appl. Mech.*, **49**, No. 4, 388–455 (2013).
63. Yu. V. Kokhanenko, "Numerical study of three-dimensional stability problems for laminated and ribbon-reinforced composites," *Int. Appl. Mech.*, **37**, No. 3, 317–345 (2001).
64. O. Lourie, D. M. Cox, and H. D. Wagner, "Buckling and collapse of embedded carbon nanotubes," *Phys. Rev. Letters*, **81**, No. 8, 1638–1641 (1998).
65. "Micromechanics of composite materials: Focus on Ukrainian research," *Appl. Mech. Rev.*, **45**, Special issue, 13–101 (1992).
66. M. R. Pinnel and F. Lawley, "Correlation on uniaxial yielding and substructure in aluminium–stainless steel composites," *Metall. Trans.*, **1**, No. 5, 929–933 (1970).
67. B. W. Rosen, "Mechanics of composite strengthening," in: *Fiber Composite Materials*, American Society for Metals, Metals Park, Ohio (1965), pp. 37–75.
68. M. A. Sadovsky, S. L. Pu, and M. A. Hussain, "Buckling of microfibers," *J. Appl. Mech.*, **34**, No. 4, 295–302 (1967).
69. Satish Kumar, Tensuya Uchida, Thuy Dang, Xiefei Zhang, and Young-Bin Park, "Polymer/carbon nano fiber composite fibers," SAMPE-2004, Long Beach, CA, May 16–20 (2004).
70. H. Schuerch, "Prediction of compressive strength in uniaxial boron fiber metal matrix composite material," *AIAA J.*, **4**, No. 1, 102–106 (1966).
71. H. R. Shetty and T. W. Chou, "Mechanical-properties and failure characteristics of FP-aluminum and W-aluminum composites," *Metall. Trans. A*, **16**, No. 5, 853–864 (1985).
72. C. Soutis, N. A. Flek, and P. A. Smith, "Failure prediction technique for compression loaded carbon fibre-epoxy laminate with open holes," *J. Comp. Mat.*, **25**, 1476–1498 (1991).
73. E. T. Thostenson and T. W. Chou, "Nanotube buckling in aligned multi-wall carbon nanotube composites," *Carbon*, **42**, No. 14, 3015–3018 (2004).
74. M. A. Wadee, G. W. Hunt, and M. A. Peletier, "Kink band instability in layered structures," *J. Mech. Phys. Solids*, **52**, 1071–1091 (2004).